Outer forearc high control in an erosional subduction regime: The case of the central Peruvian forearc (6–10°S)

Marie-Catherine Genge, César Witt, Frank Chanier, Jean-Yves Reynaud, Ysabel Calderon

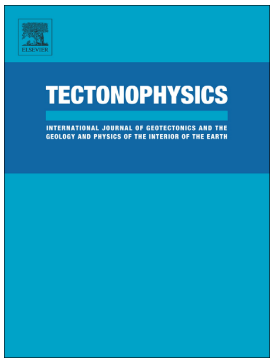

Outer forearc high control in an erosional subduction regime: The case of the central Peruvian forearc (6–10°S)

Marie Catherine Genge, César Witt, Frank Chanier, Jean-Yves Reynaud, Ysabel Calderon

PII: S0040-1951(20)30229-8

DOI: https://doi.org/10.1016/j.tecto.2020.228546

Reference: TECTO 228546

To appear in: *Tectonophysics*

Received date: 7 April 2020

Revised date: 10 June 2020

Accepted date: 17 June 2020

Please cite this article as: M.C. Genge, C. Witt, F. Chanier, et al., Outer forearc high control in an erosional subduction regime: The case of the central Peruvian forearc (6–10°S), *Tectonophysics* (2019), https://doi.org/10.1016/j.tecto.2020.228546

Outer forearc high control in an erosional subduction regime: the case of the central Peruvian forearc (6-10°S)

Marie Catherine Genge[1,2], César Witt[1], Frank Chanier[1], Jean-Yves Reynaud[1], Ysabel Calderon[3]

1: Univ. Lille, CNRS, Univ. Littoral Côte d'Opale, UMR 8187, LOG, Laboratoire d'Océanologie et de Géosciences, F 59000 Lille, France

2: Dipartimento di Geoscienze, Università degli Studi di Padova, via G. Gradenigo 6, 35131 Padova PD, Italy

3: Perupetro, Av. Luis Aldana 320, San Borja, Lima, Peru

Abstract

Outer forearc high control in an erosional subduction regime: the case of the central Peruvian forearc (6-10°S)

Marie Catherine Genge[1,2], César Witt[1], Frank Chanier[1], Jean-Yves Reynaud[1], Ysabel Calderon[3]

1: Univ. Lille, CNRS, Univ. Littoral Côte d'Opale, UMR 8187, LOG, Laboratoire d'Océanologie et de Géosciences, F 59000 Lille, France

2: Dipartimento di Geoscienze, Università degli Studi di Padova, via G. Gradenigo 6, 35131 Padova PD, Italy

3: Perupetro, Av. Luis Aldana 320, San Borja, Lima, Peru

Abstract

The forearc of the North-Central Peruvian Andes (FNCPA, 6-10°S) provides an exceptional opportunity to study the long-term processes that affect a convergent plate boundary. First, it shows long-term subsidence, depocenter superimposition and individualization. Second, although being mostly extensional and characterized as a typical erosive margin, the FNCPA shows complex uplifted regions. Older deformation is expressed by basement horst and grabens disposed in a complex geometry which onset may have resulted from strike-slip tectonics. A long-lived episode of regional subsidence affected the forearc and led to the relatively thick and regional deposition of the lower Miocene series coeval with a significant increase of the convergence velocity. This period was followed by an episodic uplift of trench-parallel corridors along the so-called Main Deformation Zone. Uplift ceased through the late Miocene and restarted during Pliocene and Quaternary, generating accommodation space by basin flank uplift for a forearc depocenter characterized by landward tilted strata. Significant along-strike differences in the degree of uplift resulted in either uplifting series producing sharp seaward dipping erosional surfaces or less uplifted areas covered by seawards prograding clinoforms. As a consequence of the shallow-water marine setting, the seismic strata geometry, lateral extent and thickness of the deposits for the Neogene successions in the FNCPA have been also tightly controlled by accommodation changes. Uplift is uneven along-strike

The forearc of the North-Central Peruvian Andes (FNCPA, 6-10°S) provides an exceptional opportunity to study the long-term processes that affect a convergent plate boundary. First, it shows long-term subsidence, depocenter superimposition and individualization. Second, although being mostly extensional and characterized as a typical erosive margin, the FNCPA shows complex uplifted regions. Older deformation is expressed by basement horst and grabens disposed in a complex geometry which onset may have resulted from strike-slip tectonics. A long-lived episode of regional subsidence affected the forearc and led to the relatively thick and regional deposition of the lower Miocene series coeval with a significant increase of the convergence velocity. This period was followed by an episodic uplift of trench-parallel corridors along the so-called Main Deformation Zone. Uplift ceased through the late Miocene and restarted during Pliocene and Quaternary, generating accommodation space by basin flank uplift for a forearc depocenter characterized by landward tilted strata. Significant along-strike differences in the degree of uplift resulted in either uplifting series producing sharp seaward dipping erosional surfaces or less uplifted areas covered by seawards prograding clinoforms. As a consequence of the shallow-water marine setting, the seismic strata geometry, lateral extent and thickness of the deposits for the Neogene successions in the FNCPA have been also tightly controlled by accommodation changes. Uplift is uneven along-strike independently of fault direction and closely followed the increase of the subsidence of the continental slope produced by subduction-erosion. Therefore, sediment underplating seems the most appropriate mechanism at the origin of uplift; as observed in other parts of the Peruvian and Chilean margins. Although the erosive character of the margin, the effects on basin geometry of the raised zone resemble that of typical outer forearc highs in accretionary margins such as in the Kumano basin in Japan.

1. Introduction

The forearc basins reflect the history of plate subduction. However, subsidence history in forearc basins is more complex and less predictable than in rifted continental margins and foreland basins

(Moxon and Graham, 1992; Xie and Heller, 2009). The main parameters controlling basin evolution (sediment supply and accommodation, e.g. Takano et al., 2013), are intimately controlled at the local and regional scale by a variety of factors such as the age and geometry of the subducting slab (Clift et al., 2003; Taylor et al., 2005), the friction of the down-going plate (Larroque et al., 1995), the thermal regime and the dynamic topography (Gerbault et al., 2009; Kimbrough et al., 2001), the plate kinematics and the accretional or erosional character of the subduction regime (Clift and Vannucchi, 2004; Martinod et al., 2010), among other aspects (e.g. Allmendinger and González, 2010; Gutscher and Westbrook, 2009; Strasser et al., 2009a). Vertical motion of the forearc and the sedimentary response on the trench slope at the short-term reflects the seismogenic cycle and therefore the subduction-fault activity (Bilek, 2010; Bilek et al., 2003; Melnick, 2016; Paquet et al., 2011; Pouderoux et al., 2014; Wells et al., 2003). However, the tectonic and topographic record of forearc regions at the long-term are still poorly documented.

The formation of a structural high between the trench and the volcanic arc is relatively common in margins related to a subduction-accretion regime (those related to accretionary prisms). This structural high forms the so-called 'Outer-forearc High' (OFH; Moore et al., 2007; Noda, 2016) or the 'trench-slope break' (Dickinson, 1995; Takano et al., 2013), which often represents an out-of-sequence thrust fault rooted at the plate interface. The OFH of the Nankai margin in Japan (Moore et al., 2007; Park et al., 2002; Strasser et al., 2009a; Moore et al., 2015) may represent the most studied example worldwide; although other examples in Cascadia (Pazzaglia and Brandon, 2001), Sumatra (Fisher et al., 2007), New Zealand (Buret et al., 1997b; Chanier et al., 1999; Bailleul et al., 2013) and Ecuador (Witt et al., 2019), have been documented. Among other aspects, the OFH controls the formation of the forearc basin (*sensu-strictu*) and the landward tilting of its sedimentary series, which are accompanied by basin expansion (a landward expansion of 20 km has been calculated for the Kumano basin in the Nankai forearc domain; Moore et al., 2015). This configuration restricts the forearc depocenter landward from the OFH in accretionary margins whereas, in non-accretionary (erosional) margins, the depocenter may extend trenchward up to the lower continental slope (Clift

and Vannucchi, 2004; Noda, 2016). In erosional margins, such as the Peruvian segment of the South America trench, the absence of an accretionary prism intuitively prevents the definition of a typical OFH. Nevertheless, although not defined as typical OFHs, similar structures can be found in erosional margins near the slope-break (see Noda, 2016) with near slope-break uplift being related to plate interface processes such as underplating as proposed for the Chilean margin (Clift and Hartley, 2007).

The Peruvian forearc, as most of Andean forearcs, shows widespread evidence of extensional deformation only sporadically interrupted by uplift (e.g. Aizprua et al., 2019; Hernandez et al., 2020, Hessler and Fildani, 2015; Clift et al., 2003; Clift and Hartley, 2007; Noda, 2016). Indeed, it is believed that subsidence has been active in the Peruvian margin since at least 50 m.y., locally and temporally interrupted by relatively local uplift highly asynchronous at the scale of the margin (e.g. Von Huene and Suess., 1988; Von Huene and Lallemand, 1990; Clift et al., 2003; Bourgois et al., 2007; Viveen and Schlunegger, 2018). These last authors suggest that in general, the evidences of extension are related to transgressive sedimentary units spanning from Eocene to Miocene, which are often faulted by normal and transtensional faults. At the scale of the entire Peruvian margin, extensional events have been mainly related to the subduction of the Nazca ridge and from the erosive regime of subduction (Von Huene and Suess, 1988; Bourgois et al., 2007; Viveen and Schlunegger, 2018). The Forearc of the North-Central Peruvian Andes (FNCPA; 6°-10°S, Fig. 1) was not affected by the subduction of the Nazca ridge (Hampel, 2002), thus providing an exceptional opportunity to study the controls and the evolution of the long-term vertical movements that affect a convergent plate boundary.

The present study focuses on the tectono-sedimentary evolution of the FNCPA during the Cenozoic. Reprocessed industrial time-migrated seismic profiles provided by Perupetro (Fig. 1) have been used to show the evolution of a complex fault system controlling several forearc depocenters and a structural high which is similar to an OFH as defined in accretionary settings. The seismic profiles have been interpreted to create a line-to-line mapping of structures and sedimentary bodies to constrain the tectonic forcing and the construction of the margin. Seismic interpretation shows that

the FNCPA has underwent subsidence for most of its Cenozoic history and that it exemplifies a more complex scenario than either an ideally accretionary or erosional margin, likewise highlighting the significant role of basement fabrics in controlling the Neogene structural development of the margin.

2. Geodynamic and geological setting

In-situ observations and rock dating in off-shore areas demonstrate that the basement of the FNCPA consist of a complex amalgamation of metamorphic, intrusive and volcanic rocks (Bellido et al., 2007; Winter et al., 2010). The Paleozoic basement crops out to the north of the study area (around the Illescas and the Paita Massifs at ~6°S; IM, Fig. 1) and is mainly composed of metasediments and quartzites intruded by Triassic granites and andesite-type intrusive bodies corresponding to the southern continuation of the Amotapes Massif (AM, Fig. 1, Romero et al., 2013; Witt et al., 2017). Two samples that could be dated at the San Martin 1X well and at the Macabi Island (SM and MI, Fig. 1) strongly suggest that the basement in these areas is a prolongation of the basement outcropping in the North in the Illescas and Amotapes Massifs (Romero et al., 2013). In the study area the basement was reached by the Morsa Norte 1X, the Ballena 1X and the Delfin 1X wells, where it has been mostly interpreted as a Paleozoic granitic basement (PARSEP, 2001 and references therein). South of the study zone, at the Lima Basin latitude (10-12°S), the offshore basement dated in the Lobera and Hormigas de Afuera islands represents an extension of the Grenville-age basement observed in the Arequipa Massif (Romero et al., 2013). Alternatively, a lack of Precambrian basement in the emerged part of the forearc and regional gravimetric models (Mamani et al., 2009) have been related to the presence of a continuous block of dense mafic material (no presence of continental basement) inherited from a possible late Paleozoic rifting (Polliand et al., 2005). However, as supported in the work of Romero et al. (2013) in the offshore regions of the FNCPA: 1) there is no evidence of mafic basement and 2) crystalline rocks have a significant continental signature as old as Precambrian.

Several documented features observed in the Peruvian margin are diagnostic of a subduction-erosion regime. These aspects include: a landward retreat of the trench, a forearc subsidence, a high rate of forearc basal erosion, normal faults and finally the presence of a small frontal prism (Bourgois et al., 2007; Clift and Vannucchi, 2004; Kukowski and Oncken, 2006; Von Huene et al., 2004; Von Huene and Lallemand, 1990). Alternatively, a recent model derived from similar seismic records as the ones used here, suggest that the basin architecture may be controlled by the presence of thrust faults deeply rooted in the basement (Prudhomme et al., 2019).

Near the study zone, drilling in ODP site 683 (3082 m water depth) found middle Eocene shallow water nannofossils (at ~500 m bsl) and benthic foraminifera from the upper and middle bathyal zones. The Eocene section is overlaid by a 40 to 25 Ma sedimentary hiatus. Sedimentation resumed with middle Miocene sediments showing lower bathyal paleontological assemblages (von Huene et al., 1988; Resig, 1990), thus, defining subsidence of the outer margin of about 1500 m during 15 m.y. This is in agreement with the subsidence resulting from subduction erosion in the Lima basin (sites 682 and 688; Von Huene et al., 1988; Resig, 1990; Clift et al., 2003) which found similar Eocene and Miocene paleontological assemblages.

In the FNCPA the Nazca plate plunges beneath the South American plate with an angle of ~17°-35°; although landwards, it may become almost horizontal at ~100 km from the trench to be again inclined ~30° below the Eastern Andes (Antonijevic et al., 2015; Boyd et al., 1984; Gutscher et al., 2000; Hasegawa and Sacks, 1981; James and Snoke, 1994). It has been proposed that this flat slab was initiated by the subduction of two oceanic buoyant crustal features: the Inca plateau and the Nazca ridge (Soler et al., 1989; Gutscher et al., 1999). The subduction of the Nazca ridge started between 16 Ma and 11 Ma at ~10°S and migrated progressively southward to its current position (at ~15°S) whereas the Inca plateau subduction may have begun at ~13 Ma at ~5°S and supposedly being entirely consumed by subsequent subduction (Gutscher et al., 1999; Hampel, 2002; Rosenbaum et al., 2005; Hu et al., 2016).

The FNCPA is segmented in the study area into three basins (Sechura, Salaverry and Trujillo Basins) with no clear structural limits (Azalgara, 1994; Marty, 1989; Romero et al., 2013; Thornburg and Kulm, 1981; Travis et al., 1976; Fig. 1). Indeed, these basins are bounded by diffuse structural highs, extending onshore in the Coastal Massifs of Illescas and Paita to the north (Romero et al., 2013; Witt et al., 2017), or buried in the outer shelf to the south (where it corresponds to the Salaverry-Trujillo High (Azalgara, 1994), or to the 'Outer-Shelf High' (Romero et al., 2013).

The free-air gravity anomalies show a patchy distribution of positive and negative values with a main trend roughly parallel to the trench (Fig. 2). Correlation of gravity anomalies with our seismic data confirms the close correspondence between positive anomalies and basement highs, and of negative anomalies with main depocenters. The structural corridor represented in land by the highs of Paita and Illescas extend seawards and is coincident with high positive anomalies (Fig. 2); also coincident with the Lobos de Afuera Island (LAI, Fig. 1). The trench-parallel depocenters are bounded by basement highs and are dissected along-strike. On land, the uplift of the Paita and Illescas structural highs is diachronous along the margin. In the Paita Massif, a single bedrock sample yielded a 63 ± 7 Ma age from apatite fission tracks and a 52.1 ± 1.6 Ma age from apatite (U-Th)/He (Wipf, 2006). Thermal modelling suggests that exhumation took place in two periods, the first one at ~65 ± 5 Ma and the most recent one at about 5 Ma (Eude et al., 2015; Garver et al., 2005; Wipf, 2006). Further south and along the west piedmont of the Andes, apatite fission-track and (U-Th)/He ages combined with thermal modelling suggest a regional exhumation at ~15 Ma (Eude et al., 2015; Margirier et al., 2015; Michalak et al., 2016).

3. Material and methods

The seismic profiles presented in this work were acquired by a joint venture between Ribiana and Perupetro S.A. in 1993. The seismic data from this survey has been migrated in the time domain and has been recently reprocessed (Perupetro) to improve the quality of the shallow reflections. Seismic profiles are mainly oriented NE-SW (e.g. perpendicular to the trench axis) with the exception of five

trench-parallel profiles (Figs. 1 and 2). The survey was carried out by the vessel M/V Digicon Explorer, equipped with a DSS-240 digital streamer, 4500 m length, 180 channels, 25 m group interval with the acquisition system resulting in a 60-fold coverage. Thirty-five profiles were analyzed in this study, over an average total length of ~4100 kilometers. Line penetration is 6 s (TWTT, two-way travel time) with clear reflections down to ~4 s (TWTT); because of high uncertainties no interpretation has been performed beneath this depth. Seismic Profiles were interpreted using conventional techniques in the Kingdom Suite® software. For the sake of simplicity lines are called here only by their number without the RIB93 prefix.

The top of basement has been difficult to identify only from interpretations of seismic lines, because of 1) inhomogeneous quality of reflectors at the top of the basement; 2) the absence of extensive core control of the top of the basement; 3) layered reflections near the top of the basement (metasediments?) and 4) a lack of clear seismic reflections in the deepest part of the depocenters. Consequently, we conducted a paired analysis of reflection seismic geometries and of free-air gravity anomalies via forward modelling on GM SYS Geosoft®, in order to propose a reliable location of the top of the basement in areas where the use of only seismic data was not satisfactory (see Supplementary materials).

In this study, sedimentary rock description and chronology was obtained from published paleontological records from four exploratory wells and ODP data (PARSEP, 2001; mostly based on former REPSOL internal reports; Von Huene and Suess, 1988; Suess, Von Huene et al., 1988). The Ballena 1X well (maximum depth 744 m) and Delfin 1X well (maximum depth 2459 m) drilled by Occidental in 1971, and several sites drilled during the 1986 ODP Leg 112 campaign (mostly site 684) offer stratigraphical and chronological constraints for the seismic profile 45 (Figs. 2 and 3). Similarly, the Morsa Norte 1X (maximum depth 989 m) and Lobos 1X (maximum depth 2028 m) wells, drilled by Repsol in 1999, offer stratigraphical and chronological constraints for the seismic profiles 40 and 30, respectively (Figs. 2 and 3).

4. Stratigraphic framework

The basement was reached in three of the wells shown here (Delfin 1X, Ballena 1X and Morsa Norte 1X). In these wells, the basement is overlain by a poorly studied Cenozoic succession starting generally in the middle Eocene (Fig. 3; PARSEP, 2001). The sedimentary succession from late Mesozoic to early Cenozoic strata is only observed in the Lobos 1X well (PARSEP, 2001; Sternbach et al., 2010). In this latter, Campanian and Maastrichtian series indicate depositional settings ranging from continental shelf to upper slope, while Paleocene and early Eocene units bear debris flows and turbidites indicative of a deeper setting or a steeper slope.

The Paleogene sediments found in the four industrial wells are mostly defined as fine-grained hemipelagic sediments with fauna typical of deep marine environments, locally interstratified with coarse-grained clastic facies (Lobos 1X, Morsa Norte 1X). The Oligocene is found only in Lobos 1X and Delfin 1X wells, topped by a regional unconformity that truncates the Paleogene. The definition of the sedimentary hiatus associated to this unconformity was one of the main results of the ODP Leg 112 (the IQ unconformity of Von Huene and Suess, 1988), which in site 683 ranges from 40 to 25 Ma (Von Huene and Suess, 1988). Its duration reaches a maximum where the early Miocene sediments rest on the middle Eocene, supposedly on horsts (e.g. Ballena 1X and Morsa 1X wells), whereas Oligocene sediments are preserved in grabens (e.g. Delfin 1X) and it is most likely correlatable with the IQ unconformity (Suess, Von Huene et al., 1988) related with sea level eustatic fall during upper Oligocene (Haq et al., 1987; PARSEP, 2001)..

The lower, middle and upper Miocene units are present and have been differentiated in all industrial exploratory wells. They correspond to dominant shallow-water, fine-grained carbonate facies sometimes dolomitized (PARSEP, 2001; Von Huene and Suess, 1988), contrasting with the coeval deep-water facies recorded in the Lima basin. In all wells, the uppermost part of the lower Miocene corresponds to an erosional surface (PARSEP, 2001), truncating sediments aged between 17.8 to 16.4 Ma in the Ballena 1X well (Schrader and Castañeda, 1990). In the latter Ballena 1X well the lower Miocene shows a deepening upward sequence, whereas the middle and upper Miocene successions

show a shallowing upward sequence (PARSEP, 2001). Trenchwards, a hardground layer is observed in the ODP Site 684 through the topmost layers of the upper Miocene defining the base of a sedimentary hiatus at 4.3 Ma (Von Huene and Suess, 1988). Pliocene sediments present in the Delfin 1X well and in the ODP Site 684 suggest a deposition in a water depth of ~100 m (PARSEP, 2001). At the top of the Pliocene section, there is a ~2 Ma hiatus encompassing the upper Pliocene and the Pleistocene (Resig, 1990; Suess, Von Huene et al., 1990).

5. Results from seismic interpretation and well data analysis

The seismic lines interpreted here show that the continental margin of the FNCPA is highly segmented. The eastern part of the margin is a large and flat floored platform with an average slope less than 1° and water depth of less than 375 m. To the west, the trench-slope break is clearly (Fig. 4A) or poorly (Fig. 4B) defined and delimits a deeper western domain (the upper continental slope) generally marked by chaotic reflections. The current trench-slope break develops independently of the deformed area (called here the Main Deformation Zone, MDZ) as it is located nearby the border (e.g. line 28, Fig. 4A) or in the core of the MDZ (e.g. line 33, Fig. 5A). Overall, in the study area, the FNCPA can be divided into three main longitudinal zones (Fig. 2): 1) an 'eastern depocenter' with sediment thickness up to about 2 s TWTT mostly unaffected by basement faults; 2) a central deformed zone (MDZ), defined by local basement emersion or shallow-water basement, raised reflectors and main faults deep-rooted in the basement forming grabens and half-grabens and 3) a westward continental slope, partially imaged from seismic records, and with unclear limits with the MDZ. Zones 1 and 2 have been ascribed in some previous works (e.g. Romero et al., 2013) to the Salaverry and Trujillo basins, respectively; whereas zone 3 has been ascribed in several works to the Yaquina basin or graben (e.g. Krabbenhoft et al., 2004). The MDZ defined in zone 2 is trench parallel and coincides, in the northern part of the study area, with the southern prolongation of the structural high outlined by the Illescas Massif and the Lobos de Afuera Island (Lines 28 and 30; Figs. 1, 4A and 4B).

The architecture of the margin is complex and defined by uplifted and subsided areas disposed in a complex patchy distribution in the MDZ. Main faults on the seismic profiles are difficult to correlate ubiquitously in a line-to-line basis considering the ~15 km spacing between profiles. However, it is clear that the basement structure is controlled by numerous large faults that delimitate half-grabens (e.g. F3 and F4 in line 36, Fig. 5B), grabens (e.g. F5/F6 in line 40, Fig. 6A; F6/F9 in line 42, Fig. 6B), and horsts (e.g. F6/F7 in line 40) coinciding with negative (for half-grabens and grabens) and positive (for horsts) free-air gravimetric anomalies (Fig. 2). Indeed, the gravimetric anomaly map mimics the basement structural position, especially east of the slope break where the sea-floor is flat and hence, where free-air anomalies are intrinsically related to lithological variations at depth.

In places where the top of the basement is clearly imaged from seismic lines, it is defined by a high-amplitude short wave-length irregular reflector outlining erosional structures possibly related to subaerial erosion processes (Fig. 5A). This erosive surface can be observed to the east and beneath the main depocenters of the MDZ suggesting that the major erosional episode could be as old as pre-Campanian (line 30 with chronology defined by the Lobos 1X well; Figs. 3 and 4B). Grabens and half-grabens in the MDZ show a complex distribution and may locally contain thick strata, reaching about 4km-thick on line 45 (Fig. 7A), with chaotic to parallel reflections most likely reflecting syn-sedimentary deformation. Furthermore, Paleogene series are almost entirely restricted to these grabens (Figs. 4B and 7A), with the exception of the wedge that pinches-out above the basement of the eastern depocenter where no fault activity could be observed (Figs. 4B, 5A, 7A and 7B).

Well data (see also Delfin 1X well in Fig. 7A) and line-to-line correlations suggest that younger sedimentary rocks sealing main depocenters in the MDZ are late Eocene in age north of ~8°S (e.g. line 40, Fig. 6A) and late Oligocene south of ~8°S (e.g. line 42, Fig. 6B). Indeed, the Oligocene series observed in wells pinch-out to the north and are only observed in the southern part of the studied zone. The erosional hiatuses that have been identified on top of Paleogene deposits in the wells are prominent in the MDZ, forming angular unconformities (better imaged on its corresponding zoom in the supplementary materials). The clearer of the Paleogene deformed depocenters was drilled at the

Lobos 1X well (line 30; Fig. 4B) and reached Cretaceous sedimentary rocks (see former section). Paleogene depocenters in the MDZ show few unconformities, difficult to correlate because of space between lines. One of these unconformities is observed in line 33 (better imaged on its corresponding zoom in the supplementary materials; Fig. 5A) and may represent the seawards expression of the erosional surface observed at the top of the basement, thus attesting for active subsidence after basement incision. Other minor unconformities may be also observed in line 40 (Fig. 6A).

Above the Oligocene unconformity, a relatively thick lower Miocene unit is observed over the entire study zone, except in uplifted areas. It overlies Eocene sediments (Fig. 6A), Oligocene sediments (Fig. 7A) and in the eastern depocenter, it onlaps onto the eroded basement (Fig. 7B). The onlapping character of the lower Miocene unit above the basement in the eastern depocenter suggests that these onlaps may be originated by a transgression; an aspect supported by the upward deepening character of the early Miocene series observed in the Ballena 1X well (PARSEP, 2001). In most of the seismic lines, the top of the lower Miocene is defined as a clear erosional surface (dated at circa 15 ± 2 Ma in the well Ballena 1X; see previous section) and observed on the flanks (e.g. line 30, Fig. 4B, offset ~65000) or above the core of the MDZ (line 42, Fig. 6B, offset ~45000). In the eastern depocenter this erosion surface is locally associated with strata tilted landward and responsible for the formation of apparent downlaps (tilted onlaps) above the gently dipping basement south of 8°S (e.g. line 45, Fig. 7A, offset ~60000). The tilting process is likely due to the pre-Pliocene uplift in the eastern part of the MDZ toward the west. Therefore, we consider that uplift along the MDZ coincides directly with the maximum of erosion on top of lower Miocene unit. Alternatively, the coeval erosion surfaces not related with uplift at the MDZ are most likely incision led by canyons (e.g. lines 30 and 40; Figs. 4A and 6A).

As for the top of the lower Miocene, the tops of the middle and upper Miocene series could also be identified over the whole margin except for some highly deformed areas within the core of the MDZ, where they are locally truncated. The middle and upper Miocene strata are unconformable over the lower Miocene series. The thickness and seismic facies of the middle and upper Miocene units rapidly

change along and across strike, possibly linked to the presence of submarine canyons (e.g. Fig. 6A, offset ~45000). The increasing thickness of the units toward the MDZ emphasizes a cessation (or at least the decrease) of uplift in the MDZ during middle and upper Miocene, which is also clearly appearing in the south of the study area from line 49 (Fig. 7B). It is more debatable for the lines located to the north (lines 28 and 30) as middle and upper Miocene units are tilted and truncated over the MDZ. Some paleo trench slope breaks, middle and upper Miocene in age, can be observed from line 40 (Fig. 6A) at offset 42500, 0.7 twtt (middle Miocene) and at offset 40000, 0.6 twtt (upper Miocene). The position of these slope breaks, with the upper Miocene slope break located at shallower depth, suggests subsidence of the margin without any resumption of the uplift of the MDZ in this area (Fig. 6A). Restricted subsidence to the east is also observed in thin sedimentary growth strata as the one observed in the hanging-wall of F9 on line 42 (Fig. 6B). Nevertheless, the interval between the top of the lower Miocene and the top of the upper Miocene shows no major fault-related thickness variations and defines a period of tectonic quiescence in the FNCPA (e.g. F9 in line 42, Fig. 6B). However, the late tilting of middle and upper Miocene series and the eroded top of upper Miocene deposits over the flanks and the core of the MDZ (e.g. lines 36 and 45; Figs. 5B and 7A) evidence a local renewal of the uplift of the MDZ during latest Miocene to Pliocene times.

The Plio-Quaternary reflectors form a relatively thick unit mostly observed in the eastern depocenter mainly south of 8°S (see along-strike profile in Supplementary Materials, DR2B). The Plio-Quaternary section shows a decreasing thickness over the MDZ (e.g. line 49, Fig. 7B) and is locally truncated by the present sea bottom surface as can be seen on lines 40 and 45 (Figs. 6A and 7A). The thickness of the unit attests for a main subsiding area localized in the eastern depocenter during Plio-Quaternary times. Towards the slope-break, older units have been tilted and either covered unconformably by Plio-Quaternary deposits on the continental slope (Fig. 6A), or literally truncated by a Plio-Quaternary erosion surface (Fig. 5A). This recent period is also remarkable for widespread tectonic activity evidenced by the development of numerous normal faults noticeable across the entire

margin, to the slope break (e.g. line 28, Fig. 4A) as well as the eastern depocenter (e.g. F9 line 42, Fig. 6B).

6. Discussion

The margin of the FNCPA exemplifies a predominantly extensional margin in which local uplift along the MDZ produces the individualization of a depocenter (i.e. formation of the eastern depocenter) with architecture similar to that observed in accretionary settings. Seismic records show that the Neogene evolution of the offshore part of the FNCPA can be divided into four main tectonic episodes: 1) a pre-Miocene episode resulting in graben and half-graben structures in the MDZ; 2) a regional subsidence episode during the lower Miocene; 3) a late early Miocene-Quaternary episode resulting in localized and episodic uplift which promoted the onset of basin individualization and 4) renewal of regional subsidence during Plio-Quaternary times accompanied by widespread normal faulting localized in the MDZ.

6.1 Pre-Miocene extension: strike-slip related depocenters?

Tectonic models in the Peruvian margin suggest that deformation resulting from oblique convergence may have started during the Late Cretaceous, coeval with the formation of intra-arc volcanosedimentary basins on the western flank of the Andes (Jaillard et al., 2000; Polliand et al., 2005). Dextral shear resulting from a Caribbean plate interaction has been also invoked as a deformation mechanism for the area north of 8°S (Kennan and Pindell, 2009). How the plate convergence obliquity is accommodated at the plate boundary is related to several parameters including interplate coupling, the length of the oblique subduction zone and the degree of obliquity (e.g. Jarrard, 1986; Jaillard et al., 2000; Chemenda et al., 2000; Philippon and Corti, 2016). Oblique convergence is well known to create partitioned systems across the forearc and/or backarc domains, with the development of roughly trench-parallel strike-slip faults typically segmented along hundreds

of kilometers as observed in Japan (Median Tectonic Line, Otsuki, 1992, Tsutsumi and Okada, 1996), Sumatra (McCaffrey, 1991; McCarthy and Elders, 1997), Ecuador (Alvarado et al., 2016; Witt and Bourgois, 2010; Yepes et al., 2016), among other systems.

Based on field observations, geomorphologic analysis, geophysical and borehole data, Viveen and Schlunegger (2018) suggested that pre-existing margin-parallel lineaments (which forms a margin-parallel strip from the piedmont to the coastline) were operating as right-lateral transfer faults between 47 and 28 Ma, the chronology of deformation being in accordance with the regional plate tectonic models of Somoza and Ghidella (2012). Viveen and Schlunegger (2018) proposed that former Jurassic to Cretaceous margin-parallel faults could have been reactivated in this context. In the FNCPA, the grabens formed are mostly parallel to the MDZ and are, at least partly, coeval with the deformation strip defined onshore by Viveen and Schlunegger (2018). Therefore, although it is not clear in seismic records whether graben and half-graben systems observed in the MDZ resulted from strike-slip tectonics, we consider that their depth, their complex geometry, their patchy distribution and their local extent most likely suggest a strike-slip origin, as observed in their onland counterparts. A strike-slip regime resulting from subduction partitioning may be difficult to conceal with the plate motion estimates obtained by Somoza and Ghidella (2012), which suggest that convergence was almost orthogonal in central and north Peru between 47 and 28 Ma, and hence that no partition of the subduction movement was occurring at that time. However, other models such as the one by Müller et al. (2008; see Figure 1 of Quinteros and Sobolev, 2013) or Müller et al. (2016; see Figure 1 of Fennell et al., 2018) propose a very high oblique convergence since the Late Cretaceous to Oligocene; thus better supporting the deformation style observed in onshore and offshore parts of the FNCPA.

Near trench margin parallel extensional structures may also be explained by a subduction erosion regime and by slab roll back. Slab roll back estimates exist only for the southernmost Peruvian margin (Oncken et al., 2006) whereas, although the resolution of the timing of subduction erosion processes in the margin is poor (see next section); the depocenters of the MDZ were formed before the onset of major subduction erosion of the margin. Although major strike-slip faults, those that controls the

tectonic escape of the forearc-arc sliver, are located in a roughly arc position in modern systems, it cannot be ruled-out that some strike slip systems, participating in the partitioning, may have formed near the trench. Furthermore, the present-day observed distance between the strike-slip systems and the trench (roughly 100 km) may have been reduced through time because of frontal erosion at the toe of the margin. Such trench retreat have been estimated to about 30 to 40 km at the latitude of the Lima Basin without taking in consideration the frontal erosion produced by the subduction of the Nazca ridge (Von Huene and Lallemand, 1990; Clift et al., 2003) and about 25-35 km at 23°S (Von Huene and Ranero, 2003) but has not been constrained for the FNCPA. We consider likely that a similar length of the margin (*c*. 25-40 km) has also been eroded in the FNCPA. According to the literature and worldwide examples, we assume that the pre-Miocene depocenters in the FNCPA were most likely linked to strain partitioning occurring during the Late Cretaceous due to oblique convergence (Fig. 8A). Strike-slip motion was sustained through the Paleogene as pre-existing lineaments operated as transfer faults in an oblique convergence setting as supported by plate tectonic models (Müller et al., 2008).

6.2 Early Miocene regional subsidence

A major unconformity, related with an emersion period, truncated the Paleogene sediments mostly restricted to the MDZ. It affected middle Oligocene sediments in depocenters and middle to upper Eocene sediments in structural highs. Afterwards, the onset of Miocene sedimentation also reflects a change to a shallower sedimentation in platform settings, which is similar to that observed in several segments of the margin (north Chile, northern Peru, South and Central Ecuador) that also attest for a major change in sedimentation environment between Paleogene and Miocene times, passing mostly from slope to platform environments (PARSEP, 2001; Suess, Von Huene et al., 1988; Viveen and Schlunegger, 2018; Von Huene and Suess, 1988; Witt et al., 2019). Undoubtedly, more regional work is needed to compare the sedimentation patterns along the margin, nonetheless, the transition from

deeper Paleogene to shallower lower Miocene series seems related to a regional plate-scale episode that resulted in uplift of the margin.

This major unconformity is overlain by a thick sedimentary unit (0.5 s TWTT in average) deposited along the entire study area. This large-scale deposition attests for a major change from localized pre-Oligocene strike-slip related subsidence to a regional subsidence during the early Miocene, and mainly ascribed to the transgressive nature of the unit above the basement. Widespread sedimentation during the early Miocene is in good agreement with a regional subsidence of the entire forearc domain, which may be related to the best-defined subduction erosion period observed from 15°S to 30°S, starting at least 20 m.y. ago (Clift and Hartley, 2007). Indeed, a direct relationship between large-scale and long-term forearc subsidence and the erosive regime of subduction has been proposed by several authors as a consequence of important basal erosion corresponding to a period of high convergence velocity (Clift and Vannucchi, 2004; Hussong, 1981; Jaillard and Soler, 1996; Kulm et al., 1982; Somoza, 1998; Somoza and Ghidella, 2012; von Huene et al., 2004; von Huene and Scholl, 1991; von Huene and Lallemand, 1990). Indeed, the formation of the major unconformity at the base of the shallow water sedimentation roughly coincides with a major change in the convergence velocity (from ~10 to ~15 cm/yr) between the juvenile Nazca and South American Plates (Pardo-Casas and Molnar, 1987; Somoza, 1998; Somoza and Ghidella, 2012) and a modest change of obliquity towards nearly orthogonal convergence (Müller et al., 2008; Müller et al., 2016).

6.3 Rise of the MDZ and forearc basin individualization from Neogene to Quaternary

The evidence for uplift along the MDZ is related to basin flank uplift and comes from: 1) erosion (e.g. line 42, Fig. 6B) or thickness reduction (e.g. line 49, Fig. 7B) of sedimentary units above uplifted basement; 2) differential erosion with uplifted areas being more eroded than surrounding areas (e.g. line 30, Fig. 4B); 3) raised reflectors in both sides of outcropping basement (e.g. line 28, Fig. 4A) or shallow water depth basement (e.g. lines 30 and 33, Figs. 4B and 5A) and 4) apparent down-lapping of lower Miocene reflectors on top of the basement of the eastern depocenter (e.g. lines 30, 45 and

49, Figs. 4B, 7A and 7B). Similar tilted geometries (apparent downlaps) have been described in the Kumano basin in Japan (Moore et al., 2007; Park et al., 2002; Strasser et al., 2009a, 2009b) and from the Hikurangi trench slope-basins in New-Zealand (Bailleul et al., 2013) and are also related to basin flank uplift. Although less obvious in the FNCPA, uplift is also highlighted by long wavelength diffuse deformation resulting in an antiform-like structure probably linked to small-displacement inversion of normal faults (e.g. line 36 and 45, Figs. 5B and 7A). The MDZ geometry is therefore controlled by the pre-existing strike-slip faults and related basins.

The erosional surface that topped the lower Miocene strata is observed regionally, not only in the vicinity of faulted areas. Furthermore, shallow-water shelf environments are recorded from the wells in the entire Miocene series (PARSEP, 2001). This character indicates a model in which eustatic falls maybe associated with emergence periods that could explain the appearance of the main lower-middle Miocene erosional surface and other subsequent minor unconformities. As a consequence of the shallow-water marine setting, the seismic strata geometry, lateral extent and thickness of the Neogene deposits in the FNCPA have been tightly controlled by accommodation changes. The main erosional surface on top of lower Miocene deposits is nearly coincident with the samples dated by Schrader and Castañeda (1990) between 17.8-16.4 to 14.2-12.9 Ma and matches one of the two well-known global eustatic sea-level falls occurring between ~ 16 and ~ 15 Ma (e.g. Haq et al., 1987; Kominz et al., 1998; Miller et al., 2005). The erosional processes were enhanced by eustatic fall affecting more the eastern flank of the MDZ as the localized uplift produced more significant incisions. A major erosional surface at *c*. 16 Ma has been also identified in north Peru in the offshore Tumbes basin and has been related to one of the two eustatic falls mentioned above (Aizprua et al., 2018) suggesting that the erosional surface observed in the FNCPA is a significant regional surface.

All the aspects mentioned above unable us to propose an age for the onset of the uplift to the late early Miocene – early middle Miocene (Fig. 8B). Deformation timing in the MDZ is in relatively good agreement with former seismic analysis (Kulm et al., 1982; Prudhomme et al., 2019), and with onland thermochronological records north of 8°S; which suggests a recent post late Miocene cooling

in the Illescas Massif (Wipf, 2006). South of 8°S, temperature-time models in the western Andean piedmont constrain onset of exhumation at *c.* 15 Ma (Margirier et al., 2015; Michalak et al., 2016). High shortening rates are also underlined between 17 and 8 Ma by the sequential restoration calibrated with low-thermochronological data (Eude et al., 2015).

The younger reflectors on the little deformed line 40 (Fig. 6A) and the thickening character of the middle Miocene unit toward the MDZ (e.g. line 45, Fig. 7A) clearly define a decrease or an interruption of the uplift in the studied area from the middle Miocene to the upper Miocene. However, middle and upper Miocene units appear tilted, more or less eroded in the core of the MDZ (e.g. line 40, Fig. 6A) and covered unconformably by Plio-Quaternary deposits. These observations suggest a resumption of the uplift after the deposition of the upper Miocene unit (Fig. 8C). This is in agreement with other studies suggesting that upper Miocene to Pleistocene sedimentary hiatuses observed in the well ODP 684 may be related to uplift episodes (Resig, 1990; Suess, Von Huene et al., 1990).

To the east, middle Miocene, upper Miocene and Plio-Quaternary units are deposited in the so-called eastern depocenter. The individualization of this depocenter (south of 8°S, Figs. 8B and 8C) resulted from diffuse basin flank uplift at the MDZ. The lack of evidences of normal faults in the basin and the relative stable position of the eastern depocenter through time support the assumption that the development of accommodation space in this depocenter is controlled by the uplift of the MDZ. Maximum thickness in the depocenter may have reached ~800 m (considering a 0.8 s TWTT depth and an average 2000 m/s velocity) for deposits younger than the late middle Miocene marker. A moderate tectonic subsidence may have thus accompanied the filling of this depocenter, taking into consideration that long-term eustatic variations since middle Miocene may not have exceeded 50 m, accordingly to recent, oxygen isotope-based eustatic charts (e.g. Miller et al., 2005). Similar forearc basin individualization following regional subsidence has been also observed and described in New-Zealand (Buret et al., 1997b). These authors associated the forearc subsidence to subduction-erosion and the individualization of the basin to the uplift of a structural high across the forearc domain, which is closely similar to that we observe along the FNCPA. The uplift of the MDZ seems to have

continued to recent time (especially north of 8°S) as most of the Plio-Quaternary reflectors of the eastern margin are truncated by the seafloor. The seafloor is almost flat on the shelf, and dominantly draped with conformable strata down to the slope margin, except where the latter is crossed by active canyons (Fig. 4A). At the seismic scale however, it corresponds to a surficial erosion observed along the entire Peruvian margin (Calvès et al., 2017). This indicates that the shelf is overfilled, with significant bypass to the trench slope, suggesting a sediment supply greater than the accommodation space created. Considering the dominantly flat parallel or offlap-dominated seismic layering of most units, this situation prevailed over the Neogene. The unit-bounding unconformities may have been formed during short tectonic episodes.

Overall, two main architectural styles have been synthetized after our observations in order to summarize the diverse structural geometries extended along the FNCPA (Fig. 9). The first architecture (Fig. 9A) represents mostly the structures observed north of 8°S, where the MDZ is characterized by an overall uprising of the entire sedimentary successions showing near the slope-break a sharp Plio-Quaternary erosion surface. On the contrary, south of 8°S, the series above the MDZ have been characterized by the tilting and erosion of the lower Miocene unit and more locally the presence of westward shelf progradational middle Miocene clinoforms which extend seawards from the slope-break (Fig. 9B). Nevertheless, the MDZ shows significant along-strike variations in the amount of deformation (with a minimum deformation at 8°S) resulting in either highly uplifting basement producing sharp seaward dipping erosional surfaces (weak trenchward bypass, e.g. line 30, Fig. 4B) or less uplifted areas covered by seawards prograding clinoforms (strong trenchward bypass, e.g. line 40, Fig. 6A). In both cases the MDZ has a trench-parallel axis and separates the forearc basin from the trench slope.

In subduction-accretion regimes, the OFH represents a structural high parallel to the trench, most likely related to the activity of an out-of-sequence thrust (mega splay fault for Strasser et al., 2009b) with periodical rather than constant activity (e.g. Conin et al., 2012). Its development controls the forearc configuration preventing (at least partially) the bypass of sediments to the trench, restricting

the forearc basin depocenter and tilting the sedimentary series in a landward direction (e.g. Moore et al., 2007; Moore et al., 2015; Noda, 2016). The evidences presented here attest for the development of a linear domain uplifted during the late early Miocene – early middle Miocene. This domain is similar to those observed on accretionary prisms, but characterized by a longer wavelength and more diffuse geometries. The processes responsible for uplift of the trench-parallel MDZ remain unclear, but the age of the first uplift event (mainly end of early Miocene - middle Miocene) and the location of the deformation over an inherited weakness zone, may suggest a mechanism associating seaward upper plate basal erosion and accretion with underplating beneath the MDZ, a mechanism suggested for other parts of the margin (e.g. Seely, 1979; Clift and Hartley, 2007) sharing more or less similar characteristics than the FNCPA.

7. Conclusions

The detailed study of seismic data allows reconstruction of the tectono-sedimentary evolution of the forearc of the North Central Peruvian Andes (FNCPA). The interpretation led us to propose that strike-slip depocenters were developed during the Late Cretaceous due to high convergence obliquity and subsequent partitioning along the margin. The strike-slip system developed throughout the Paleogene, forming a trench parallel corridor of transtensional structures, called here the Main Deformation Zone (MDZ). A major unconformity, affecting middle Eocene series north of ~8°S and Oligocene series south of it, seal these deposits and may represent the landward extension of the main IQ unconformity previously described from ODP drilling records. Sedimentation resumed with the widespread early Miocene series. It is plausible that the erosive subduction regime favored basal erosion generating a long-term and regional subsidence of the forearc as evidenced by the important thickness of the lower Miocene unit.

The MDZ was affected by episodic uplift during the end of the early Miocene and during the Pliocene. Uplift along the MDZ produced a tectonic setting very similar to an outer forearc high, typical of

many accretionary settings. Uplift produced the landward tilting of lower Miocene strata enhancing local erosion, generally in the axis or on the eastern flank of the MDZ as localized uplift coeval with eustatic falls in a shelf environment produce more significant erosion. The local thickening of the middle and upper Miocene units in the core of the deformed area (MDZ) indicates uplift interruption. Resumption of the uplift is noticed after the deposition of upper Miocene sediments which induced the development of a depocenter to the east. The individualization of such a forearc basin (i.e. the eastern depocenter) resulting from the formation of a seaward structural high is generally typical from accretionary margins. Our study shows that this particular type of basin can also develop along active margins that are characterized by an erosional tectonic regime.

The patchy distribution and complex geometry of depocenters and structural highs observed along the FNCPA can result from the interaction between pre-existing strike-slip faults and related basins and subsequent basin flank uplift. Uplift activity seems to closely follow the onset of the erosional subduction regime in the margin. Therefore the spatial distribution and timing of uplift, as well as the tectonic evolution of the margin, bring us to propose that basal underplating is the most likely process to account for the episodic uplift episodes observed in the FNCPA.

Acknowledgements

We kindly thank Perupetro for helping us to get access to the data used in this work. This study was financed by the INSU (Institut National des Sciences de l'Univers, France) through a Telus-Syster scholarship accorded to CW. We thank Jacky Ferrière, Kiko Valencia and Darwin Romero for helpful discussions that helped to construct this manuscript. We thank E. Jaillard for his constructive review that helped us to improve the quality of the paper. We would also like to thank IHS for the academic license of the Kingdom suite software.

References

Aizprua, C., Witt, C., Johansen, S. E., & Barba, D., 2019. Cenozoic Stages of Forearc Evolution Following the Accretion of a Sliver From the Late Cretaceous-Caribbean Large Igneous Province: SW Ecuador-NW Peru. Tectonics, 38(4), 1441-1465.

Allmendinger, R.W., González, G., 2010. Invited review paper: Neogene to Quaternary tectonics of the coastal Cordillera, northern Chile. Tectonophysics 495, 93–110.

Alvarado, A., Audin, L., Nocquet, J.M., Jaillard, E., Mothes, P., Jarrín, P., Segovia, M., Rolandone, F., Cisneros, D., 2016. Partitioning of oblique convergence in the Northern Andes subduction zone: Migration history and the present-day boundary of the North Andean Sliver in Ecuador. Tectonics 35, 1048–1065. https://doi.org/10.1002/2016TC004117

Antonijevic, S.K., Wagner, L.S., Kumar, A., Beck, S.L., Long, M.D., Zandt, G., Tavera, H., Condori, C., 2015. The role of ridges in the formation and longevity of flat slabs. Nature 524, 212–215.

Azalgara, C., 1994. Structural evolution of the offshore forearc basins of Peru, including the Salaverry, Trujillo, Lima, West Pisco and East Pisco basins. Rice University.

Bailleul, J., Chanier, F., Ferrière, J., Robin, C., Nicol, A., Mahieux, G., Gorini, C., Caron, V., 2013. Neogene evolution of lower trench-slope basins and wedge development in the central Hikurangi subduction margin, New Zealand. Tectonophysics 591, 152–174.

Bellido F., P. Valverde, F. Jaimes, V. Carlotto, E. Díaz-Martínez, 2007. Datación y caracterización geoquímica de los granitoides peralumínicos de los cerros de Amotape y de los Macizos de Illescas y Paita (Noroeste de Perú). Boletín Sociedad Geológica del Perú, 103, pp. 197-213.

Bilek, S.L., 2010. Invited review paper: Seismicity along the South American subduction zone: Review of large earthquakes, tsunamis and subduction zone complexity. Tectonophysics 495, 2–14.

Bilek, S.L., Schwartz, S.Y., DeShon, H.R., 2003. Control of seafloor roughness on earthquake rupture behavior. Geology 31, 455–458.

Bourgois, J., Bigot Cormier, F., Bourles, D., Braucher, R., Dauteuil, O., Witt, C., Michaud, F., 2007. Tectonic record of strain buildup and abrupt coseismic stress release across the northwestern Peru coastal plain, shelf, and continental slope during the past 200 kyr-art. no. B04104. J. Geophys. Res. Solid Earth 112, NIL_46–NIL_67.

Boyd, T.M., Snoke, J.A., Sacks, I.S., Rodriguez B, A., 1984. High-resolution determination of the Benioff zone geometry beneath southern Peru. Bull. Seismol. Soc. Am. 74, 559–568.

Buret, C., Chanier, F., Ferrière, J., Proust, J.-N., 1997b. Individualization of a forearc basin during the active margin evolution: Hikurangi subduction margin, New Zealand. Comptes Rendus Acad. Sci. Ser. IIA Earth Planet. Sci. 8, 615–621.

Calvès, G., Auguy, C., De Lavaissière, L., Brusset, S., Calderon, Y., & Baby, P., 2017. Fore-arc seafloor unconformities and geology: Insight from 3-D seismic geomorphology analysis, Peru. Geochemistry, Geophysics, Geosystems, 18(8), 3062-3077.

Chanier, F., Ferrière, J., & Angelier, J., 1999. Extensional deformation across an active margin, relations with subsidence, uplift and rotations: The Hikurangi subduction, New Zealand. Tectonics, vol. 18, 862-876.

Chemenda, A., Lallemand, S., & Bokun, A., 2000. Strain partitioning and interplate friction in oblique subduction zones: Constraints provided by experimental modeling. Journal of Geophysical Research: Solid Earth, 105(B3), 5567-5581.

Clift, P., Vannucchi, P., 2004. Controls on tectonic accretion versus erosion in subduction zones: Implications for the origin and recycling of the continental crust. Rev. Geophys. 42.

Clift, P.D., Hartley, A.J., 2007. Slow rates of subduction erosion and coastal underplating along the Andean margin of Chile and Peru. Geology 35, 503–506.

Clift, P.D., Pecher, I., Kukowski, N., Hampel, A., 2003. Tectonic erosion of the Peruvian forearc, Lima Basin, by subduction and Nazca Ridge collision. Tectonics 22.

Conin, M., Henry, P., Godard, V., Bourlange, S., 2012. Splay fault slip in a subduction margin, a new model of evolution. Earth Planet. Sci. Lett. 341–344, 170–175. https://doi.org/10.1016/j.epsl.2012.06.003

DeMets, C., Gordon, R.G., Argus, D.F., Stein, S., 1994. Effect of recent revisions to the geomagnetic reversal time scale on estimates of current plate motions. Geophys. Res. Lett. 21, 2191–2194.

Dickinson, W.R., 1995, Forearc basins, in Busby, C.J., and Ingersoll, R.V., eds., Tectonics of Sedimentary Basins: Cambridge, Massachusetts, Blackwell Science, p. 221–261.

Eude, A., Roddaz, M., Brichau, S., Brusset, S., Calderon, Y., Baby, P., & Soula, J. C., 2015. Controls on timing of exhumation and deformation in the northern Peruvian eastern Andean wedge as inferred from low-temperature thermochronology and balanced cross section. Tectonics, 34(4), 715-730.

Fennell, L. M., Quinteros, J., Iannelli, S. B., Litvak, V. D., & Folguera, A. (2018). The role of the slab pull force in the late Oligocene to early Miocene extension in the Southern Central Andes (27-46 S): Insights from numerical modeling. Journal of South American Earth Sciences, 87, 174-187.

Fisher, D., Mosher, D., Austin, J.A., Gulick, S.P.S., Masterlark, T., Moran, K., 2007. Active deformation across the Sumatran forearc over the December 2004 Mw9.2 rupture. Geology 35, 99–102. https://doi.org/10.1130/G22993A.1

Garver, J. I., Reiners, P. W., Walker, L. J., Ramage, J. M., & Perry, S. E., 2005. Implications for timing of Andean uplift from thermal resetting of radiation-damaged zircon in the Cordillera Huayhuash, northern Peru. The Journal of Geology, 113(2), 117-138.

Gerbault, M., Cembrano, J., Mpodozis, C., Farias, M., Pardo, M., 2009. Continental margin deformation along the Andean subduction zone: Thermo-mechanical models. Phys. Earth Planet. Inter. 177, 180–205.

Gutscher, M.-A., Olivet, J.-L., Aslanian, D., Eissen, J.-P., Maury, R., 1999. The "lost Inca Plateau": cause of flat subduction beneath Peru? Earth Planet. Sci. Lett. 171, 335–341.

Gutscher, M.-A., Spakman, W., Bijwaard, H., Engdahl, E.R., 2000. Geodynamics of flat subduction: Seismicity and tomographic constraints from the Andean margin. Tectonics 19, 814–833.

Gutscher, M.-A., Westbrook, G.K., 2009. Great earthquakes in slow-subduction, low-taper margins, in: Subduction Zone Geodynamics. Springer, pp. 119–133.

Hampel, A., 2002. The migration history of the Nazca Ridge along the Peruvian active margin: a re-evaluation. Earth Planet. Sci. Lett. 203, 665–679.

Haq, B. U., Hardenbol, J. A. N., & Vail, P. R., 1987. Chronology of fluctuating sea levels since the Triassic. Science, 235(4793), 1156-1167.Hartley, A. J., & Evenstar, L., 2010. Cenozoic stratigraphic development in the north Chilean forearc: Implications for basin development and uplift history of the Central Andean margin. Tectonophysics, 495(1-2), 67-77.

Hasegawa, A., Sacks, I.S., 1981. Subduction of the Nazca plate beneath Peru as determined from seismic observations. J. Geophys. Res. Solid Earth 86, 4971–4980.

Hernández, M. J., Michaud, F., Collot, J. Y., Proust, J. N., & d'Acremont, E., 2020. Evolution of the Ecuador offshore nonaccretionary forearc basin and margin segmentation. Tectonophysics, 228374.

Hessler, A. M., & Fildani, A., 2015. Andean forearc dynamics, as recorded by detrital zircon from the Eocene Talara Basin, northwest Peru. Journal of Sedimentary Research, 85(6), 646-659.

Hu, J., Liu, L., Hermosillo, A., & Zhou, Q., 2016. Simulation of late Cenozoic South American flat-slab subduction using geodynamic models with data assimilation. Earth and Planetary Science Letters, 438, 1-13.

Jaillard, E., Hérail, G., Monfret, T., Díaz-Martínez, E., Baby, P., Lavenu, A., & Dumont, J. F., 2000. Tectonic evolution of the Andes of Ecuador, Peru, Bolivia and northernmost Chile. Tectonic Evolution of South America, 31, 481-559.

Jaillard, E., & Soler, P., 1996. Cretaceous to early Paleogene tectonic evolution of the northern Central Andes (0–18 S) and its relations to geodynamics. Tectonophysics, 259(1-3), 41-53.

James, D.E., Snoke, J.A., 1994. Structure and tectonics in the region of flat subduction beneath central Peru: Crust and uppermost mantle. J. Geophys. Res. Solid Earth 99, 6899–6912.

Jarrard, R. D., 1986. Relations among subduction parameters. Reviews of Geophysics, 24(2), 217-284.

Kennan, L., & Pindell, J. L., 2009. Dextral shear, terrane accretion and basin formation in the Northern Andes: best explained by interaction with a Pacific-derived Caribbean Plate?. Geological Society, London, Special Publications, 328(1), 487-531.

Kimbrough, D.L., Smith, D.P., Mahoney, J.B., Moore, T.E., Grove, M., Gastil, R.G., Ortega-Rivera, A., Fanning, C.M., 2001. Forearc-basin sedimentary response to rapid Late Cretaceous batholith emplacement in the Peninsular Ranges of southern and Baja California. Geology 29, 491–494.

Kominz, M. A., Miller, K. G., & Browning, J. V., 1998. Long-term and short-term global Cenozoic sea-level estimates. Geology, 26(4), 311-314.

Krabbenhöft, A., Bialas, J., Kopp, H., Kukowski, N., Hübscher, C., 2004. Crustal structure of the Peruvian continental margin from wide-angle seismic studies. Geophys. J. Int. 159, 749–764.

Kukowski, N., Oncken, O., 2006. Subduction Erosion—the "Normal" Mode of Fore-Arc Material Transfer along the Chilean Margin?, in: The Andes. Springer, pp. 217–236.

Kulm, L. D., Thornburg, T. M., Schrader, H. J., & Resig, J. M., 1982. Cenozoic structure, stratigraphy and tectonics of the central Peru forearc. Geological Society, London, Special Publications, 10(1), 151-169.

Larroque, C., Calassou, S., Malavieille, J., & Chanier, F., 1995. Experimental modelling of forearc basin development during accretionary wedge growth. Basin Research, 7(3), 255-268.

Mamani, M., Carlotto, V., Santos, A., Acosta, H., Rodríguez, R., Martiarena, R., Rodriguez, J., Navarro, J., Cacya, L., Alvan, A., Cornejo, T., Peña, D., Aguilar, R. (2009). Resultados de la interpolación regional de las anomalías de Bouguer y su correlación con los dominios geotectónicos del Perú. Bol. Soc. Geol. Perú, 103, 255-263.

Margirier, A., Robert, X., Audin, L., Gautheron, C., Bernet, M., Hall, S., Simon-Labric, T., 2015. Slab flattening, magmatism, and surface uplift in the Cordillera Occidental (northern Peru). Geology 43, 1031–1034.

Martinod, J., Husson, L., Roperch, P., Guillaume, B., Espurt, N., 2010. Horizontal subduction zones, convergence velocity and the building of the Andes. Earth Planet. Sci. Lett. 299, 299–309.

Marty, R.C., 1989. Stratigraphy and chemical sedimentology of Cenozoic biogenic sediments from the Pisco and Sechura basins, Peru (PhD Thesis). Rice University.

McCaffrey, R., 1991. Slip vectors and stretching of the Sumatran fore arc. Geology, 19(9), 881-884.

McCarthy, A. J., & Elders, C. F., 1997. Cenozoic deformation in Sumatra: oblique subduction and the development of the Sumatran Fault System. Geological Society, London, Special Publications, 126(1), 355-363.

Melnick, D., 2016. Rise of the central Andean coast by earthquakes straddling the Moho. Nature Geoscience, 9(5), 401.Michalak, M. J., Hall, S. R., Farber, D. L., Audin, L., & Hourigan, J. K., 2016. (U-Th)/He thermochronology records late Miocene accelerated cooling in the north-central Peruvian Andes. Lithosphere, 8(2), 103-115.

Michalak, M. J., Hall, S. R., Farber, D. L., Audin, L., & Hourigan, J. K., 2016. (U-Th)/He thermochronology records late Miocene accelerated cooling in the north-central Peruvian Andes. Lithosphere, 8(2), 103-115.

Miller, K. G., Kominz, M. A., Browning, J. V., Wright, J. D., Mountain, G. S., Katz, M. E., Sugarman, P. J., Cramer, B. S., Christie-Blick N., Pekar, S. F., 2005. The Phanerozoic record of global sea-level change. science, 310(5752), 1293-1298.

Moore, G.F., Bangs, N.L., Taira, A., Kuramoto, S., Pangborn, E., Tobin, H.J., 2007. Three-dimensional splay fault geometry and implications for tsunami generation. Science 318, 1128–1131.

Moore, G.F., Boston, B.B., Strasser, M., Underwood, M.B., Ratliff, R.A., 2015. Evolution of tectono-sedimentary systems in the Kumano Basin, Nankai Trough forearc. Mar. Pet. Geol. 67, 604–616. https://doi.org/10.1016/j.marpetgeo.2015.05.032

Moxon, I.W., Graham, S.A., 1992. History and controls of subsidence in the Late Cretaceous-Tertiary Great Valley forearc basin, California, 1-4.

Müller, R. D., Sdrolias, M., Gaina, C., & Roest, W. R., 2008. Age, spreading rates, and spreading asymmetry of the world's ocean crust. Geochemistry, Geophysics, Geosystems, 9(4).

Müller, R. D., Seton, M., Zahirovic, S., Williams, S. E., Matthews, K. J., Wright, N. M., Shepard, G. E., Maloney, K. T., Barnett-Moore, N., Hosseinpour, M., Bower, D. J., & Cannon, J., 2016. Ocean basin evolution and global-scale plate reorganization events since Pangea breakup. Annual Review of Earth and Planetary Sciences, 44, 107-138.

Noble, D. C., McKEE, E. H., Mourier, T., & Mégard, F., 1990. Cenozoic stratigraphy, magmatic activity, compressive deformation, and uplift in northern Peru. Geological Society of America Bulletin, 102(8), 1105-1113.

Noda, A., 2016. Forearc basins: Types, geometries, and relationships to subduction zone dynamics. Geol. Soc. Am. Bull. 128, 879–895.

Oncken, O., Hindle, D., Kley, J., Elger, K., Victor, P., & Schemmann, K., 2006. Deformation of the central Andean upper plate system—Facts, fiction, and constraints for plateau models. In The Andes (pp. 3-27). Springer, Berlin, Heidelberg.

Otsuki, K., 1992. Oblique subduction, collision of microcontinents and subduction of oceanic ridge: their implications on the Cretaceous tectonics of Japan. Island Arc, 1(1), 51-63.

Paquet, F., Proust, J.-N., Barnes, P.M., Pettinga, J.R., 2011. Controls on active forearc basin stratigraphy and sediment fluxes: The Pleistocene of Hawke Bay, New Zealand. GSA Bull. 123, 1074–1096.

Pardo-Casas, F., & Molnar, P., 1987. Relative motion of the Nazca (Farallon) and South American plates since Late Cretaceous time. Tectonics, 6(3), 233-248.

Park, J.-O., Tsuru, T., Kodaira, S., Cummins, P.R., Kaneda, Y., 2002. Splay fault branching along the Nankai subduction zone. Science 297, 1157–1160.

PARSEP (2001) - Torres, J, and Fontecha, B.; Stratigraphy and sedimentology of wells Morsa Norte Z29M-37-1X and Lobos Z29M-9-1X.

Pazzaglia, F.J., Brandon, M.T., 2001. A Fluvial Record of Long-term Steady-state Uplift and Erosion Across the Cascadia Forearc High, Western Washington State. Am. J. Sci. 301, 385–431. https://doi.org/10.2475/ajs.301.4-5.385

Philippon, M., & Corti, G., 2016. Obliquity along plate boundaries. Tectonophysics, 693, 171-182.

Polliand, M., Schaltegger, U., Frank, M., Fontbote, L., 2005. Formation of intra-arc volcanosedimentary basins in the western flank of the central Peruvian Andes during Late Cretaceous oblique subduction: field evidence and constraints from U–Pb ages and Hf isotopes. Int. J. Earth Sci. 94, 231–242.

Pouderoux, H., Proust, J.-N., Lamarche, G., 2014. Submarine paleoseismology of the northern Hikurangi subduction margin of New Zealand as deduced from turbidite record since 16 ka. Quat. Sci. Rev. 84, 116–131.

Prudhomme, A., Baby, P., Robert, A., Brichau, S., Cuipa, E., Eude, A., Calderon Y., O'Sullivan, P., 2019. Western thrusting and uplift in northern Central Andes (western Peruvian margin). In Andean Tectonics (pp. 299-331). Elsevier.

Quinteros, J., & Sobolev, S. V., 2013. Why has the Nazca plate slowed since the Neogene?. Geology, 41(1), 31-34.

Resig, J.M., 1990. Benthic foraminiferal stratigraphy and paleoenvironments off Peru, Leg 112, in: Proceedings of the Ocean Drilling Program, Scientific Results. pp. 263–296.

Romero, D., Valencia, K., Alarcón, P., Peña, D., Ramos, V.A., 2013. The offshore basement of Perú: Evidence for different igneous and metamorphic domains in the forearc. J. South Am. Earth Sci. 42, 47–60.

Rosenbaum, G., Giles, D., Saxon, M., Betts, P.G., Weinberg, R.F., Duboz, C., 2005. Subduction of the Nazca Ridge and the Inca Plateau: Insights into the formation of ore deposits in Peru. Earth Planet. Sci. Lett. 239, 18–32.

Sandwell, D.T., Smith, W.H.F., 1997. Marine gravity anomaly from Geosat and ERS 1 satellite altimetry. J. Geophys. Res. Solid Earth 102, 10039–10054. https://doi.org/10.1029/96JB03223

Schrader, H., & Castaneda, J. C., 1990. 13. THE BALLENA AND DELFIN WELLS OFF CENTRAL PERU: REVISED AGES1. In Proceedings of the ocean drilling program: Scientific Results (p. 209). The Program.

Seely, D. R. (1979). The Evolution of Structural Highs Bordering Major Forearc Basins: Convergent Margins.

Soler, P., Carlier, G., & Marocco, R., 1989. Evidence for the subduction and underplating of an oceanic plateau beneath the south Peruvian margin during the late Cretaceous: structural implications. Tectonophysics, 163(1-2), 13-24.

Somoza, R., 1998. Updated Nazca (Farallon)—South America relative motions during the last 40 My: implications for mountain building in the central Andean region. J. South Am. Earth Sci. 11, 211–215.

Somoza, R., Ghidella, M.E., 2012. Late Cretaceous to recent plate motions in western South America revisited. Earth Planet. Sci. Lett. 331, 152–163.

Sternbach, L. R., Bang, S., Bianchi, C., Cespedes, J., Han, Y., & Choi, D. S., 2010. PS Offshore Peru, Trujillo Basin, Block Z-46: 2D PSTM Seismic Processing Reveals Deep Basins, Normal and Trans-Tensional Faulting, and Thick Eocene/Oligocene Stratigraphically Complex Submarine Fans Linked to Evidence of Hydrocarbons/DHIs.

Strasser, M., Moore, G.F., Kimura, G., Kitamura, Y., Kopf, A.J., Lallemant, S., Park, J.-O., Screaton, E.J., Su, X., Underwood, M.B., others, 2009a. Origin and evolution of a splay fault in the Nankai accretionary wedge. Nat. Geosci. 2, 648–652.

Strasser, M., Moore, G.F., Kimura, G., Kitamura, Y., Kopf, A.J., Lallemant, S., Park, J.-O., Screaton, E.J., Su, X., Underwood, M.B., Zhao, X., 2009b. Origin and evolution of a splay fault in the Nankai accretionary wedge. Nat. Geosci. 2, 648–652. https://doi.org/10.1038/ngeo609

Suess, E., Von Huene, R., 1988. Ocean Drilling Program Leg 112, Peru continental margin: Part 2, Sedimentary history and diagenesis in a coastal upwelling environment. Geology 16, 939–943.

Suess, E., Von Huene, R., et al., 1988. Shipboard Scientific Party, 1988. Site 684., in: Proceedings of Ocean Drilling Program, Leg 112 Initial Reports, Part A: College Station, TX (Ocean Drilling Program). pp. 525–595.

Suess, E., Von Huene, R., others, A. 26, 1990. Proceedings of the Ocean Drilling Program, Vol. 112, Scientific Results, Peru Continental Margin. Ocean Drilling Program.

Takano, O., Itoh, Y., & Kusumoto, S., 2013. Variation in forearc basin configuration and basin-filling depositional systems as a function of trench slope break development and strike-slip movement: Examples from the Cenozoic Ishikari-Sanriku-Oki and Tokai-Oki-Kumano-Nada forearc basins, Japan. Mechanism of Sedimentary Basin Formation: Multidisciplinary Approach on Active Plate Margins,, 3-25.

Taylor, F.W., Mann, P., Bevis, M.G., Edwards, R.L., Cheng, H., Cutler, K.B., Gray, S.C., Burr, G.S., Beck, J.W., Phillips, D.A., others, 2005. Rapid forearc uplift and subsidence caused by impinging bathymetric features: Examples from the New Hebrides and Solomon arcs. Tectonics 24(6).

Thornburg, T. M., & Kulm, L. D., 1981. Sedimentary basins of the Peru continental margin: Structure, stratigraphy, and Cenozoic tectonics from 6 S to 16 S latitude. Geological Society of America Memoir, 154, 393-422.

Travis, R.B., Gonzales, G., Pardo, A., 1976. Hydrocarbon Potential of Coastal Basins of Peru: Hydrocarbons. pp. 331–338.

Tsutsumi, H., & Okada, A., 1996. Segmentation and Holocene surface faulting on the Median Tectonic Line, southwest Japan. Journal of Geophysical Research: Solid Earth, 101(B3), 5855-5871.

Viveen, W., Schlunegger, F., 2018. Prolonged extension and subsidence of the Peruvian forearc during the Cenozoic. Tectonophysics 730, 48–62. https://doi.org/10.1016/j.tecto.2018.02.018

Von Huene, R., Lallemand, S., 1990. Tectonic erosion along the Japan and Peru convergent margins. Geol. Soc. Am. Bull. 102, 704–720.

Von Huene, R. Ranero, C.R., 2003. Subduction erosion and basal friction along the sediment-starved convergent margin off Antofagasta, Chile. J. Geophys. Res. Solid Earth 108. https://doi.org/10.1029/2001JB001569

Von Huene, R., Ranero, C.R., Vannucchi, P., 2004. Generic model of subduction erosion. Geology 32, 913–916.

Von Huene, R., & Scholl, D. W., 1991. Observations at convergent margins concerning sediment subduction, subduction erosion, and the growth of continental crust. Reviews of Geophysics, 29(3), 279-316.

Von Huene, R., Suess, E., 1988. Ocean Drilling Program Leg 112, Peru continental margin: part 1, tectonic history. Geology 16, 934–938.

Wells, R.E., Blakely, R.J., Sugiyama, Y., Scholl, D.W., Dinterman, P.A., 2003. Basin-centered asperities in great subduction zone earthquakes: A link between slip, subsidence, and subduction erosion? J. Geophys. Res. Solid Earth 108(10).

Winter, L. S., Tosdal, R. M., Mortensen, J. K., & Franklin, J. M. (2010). Volcanic stratigraphy and geochronology of the Cretaceous Lancones Basin, northwestern Peru: Position and timing of giant VMS deposits. Economic Geology, 105(4), 713-742.

Wipf, M.A., 2006. Evolution of the Western Cordillera and coastal margin of Peru: evidence from low-temperature thermochronology and geomorphology.

Witt, C., Bourgois, J., 2010. Forearc basin formation in the tectonic wake of a collision-driven, coastwise migrating crustal block: The example of the North Andean block and the extensional Gulf of Guayaquil-Tumbes Basin (Ecuador-Peru border area). Geol. Soc. Am. Bull. 122, 89–108. https://doi.org/10.1130/b26386.1

Witt, C., Reynaud, J.Y., Barba, D., Poujol, M., Aizprua, C., Rivadeneira, M., Amberg, C., 2019. From accretion to forearc basin initiation: The case of SW Ecuador, Northern Andes. Sediment. Geol. https://doi.org/10.1016/j.sedgeo.2018.11.009

Witt, C., Rivadeneira, M., Poujol, M., Barba, D., Beida, D., Beseme, G., Montenegro, G., 2017. Tracking ancient magmatism and Cenozoic topographic growth within the Northern Andes forearc: Constraints from detrital U-Pb zircon ages. Geol. Soc. Am. Bull. 129(3–4). pp. 415–428

Xie, X., Heller, P.L., 2009. Plate tectonics and basin subsidence history. Geol. Soc. Am. Bull. 121, 55–64.

Yepes, H., Audin, L., Alvarado, A., Beauval, C., Aguilar, J., Font, Y., Cotton, F., 2016. A new view for the geodynamics of Ecuador: Implication in seismogenic source definition and seismic hazard assessment. Tectonics 35, 1249–1279. https://doi.org/10.1002/2015TC003941

Figures

Fig. 1. Geodynamic sketch of North and Central Peru showing the location of seismic lines used in this study. Black circles show ODP sites from Leg 112 and 201 (sites' number indicated on the map). Yellow hexagons show industrial well sites (B: Ballena 1X, D: Delfin 1X, L: Lobos 1X, MN: Morsa Norte 1X). Red rectangles

refer to obtained basement ages discussed in the text (AM: Amotapes Massif, HAI: Homigas de Afuera Island, IM: Illescas Massif, LAI: Lobos de Afuera Island, LI: Lobera Island, MI: Macabi Island, SM: San Martin 1X). Basins boundaries were obtained from Perupetro. Plate ages obtained from Müller et al. (1997). Current plate motion estimated from the Nazca-South America convergence pole of the NUVEL-1 global plate of motion model (DeMets et al., 1994). Topography and bathymetry from GeoMapApp.

Fig. 2. Gravity map (Sandwell and Smith, 1997) from GeoMapApp (resolution: 1,75 km²) with the position of seismic lines interpreted in this study and wells used for chronology purposes (PARSEP, 2001). Faults are located after seismic interpretation.

Fig. 3. Log of wells used for stratigraphic correlation and basement top location (Suess, Von Huene et al., 1990; Suess and Von Huene, 1988; PARSEP, 2001).

Fig. 4. A. Seismic profile RIB93-28. Note the erosional slope and the near-edge basement horst. The units are folded against the faults, with an upward decreasing dip. **B.** Seismic profile RIB93-30. The basement high is buried below tilted Paleogene units covered unconformably by Plio-Quaternary deposits near the surface. Dotted square indicates the area zoomed in the supplementary materials (DR4A). See location in Fig. 2. Corresponding non-interpreted seismic profiles in supplementary materials (DR6).

Fig. 5. A. Seismic profile RIB93-33. The basement high is buried by Paleogene units below a major unconformity. Neogene deposits related with a transgression onlap the basement landward. Dotted square indicates the area zoomed in the supplementary materials (DR4B). **B.** Seismic profile RIB93-36. The basement high has a lower amplitude and is buried under Cenozoic deposits. See location in Fig. 2. Corresponding non-interpreted seismic profiles in supplementary materials (DR7).

Fig. 6. A. Seismic profile RIB93-40. Lower Miocene top is eroded and filled by middle and upper Miocene prograding deposits. Lower Miocene strata form apparent downlaps along the basement landward. Dotted square indicates the area zoomed in the supplementary materials (DR5A). **B.** Seismic profile RIB93-42. The fault F9 was active recently as evidence by the different thickness of Plio-Quaternary deposits on both side of the faults. FMDBL: Forward Modeling Inverse-Derived Basement Location (see Supplementary materials DR1). See location in Fig. 2. Corresponding non-interpreted seismic profiles in supplementary materials (DR8).

Fig. 7. A. Seismic profile RIB93-45. Graben inverted during the Neogene. Landward Plio-Quaternary reflectors are tilted close to the MDZ and truncated by the current seafloor. FMDBL: Forward Modeling Inverse-Derived Basement Location (see Supplementary materials). Dotted square indicates the area zoomed in the supplementary materials (DR5B). **B.** Seismic profile RIB93-49. Lower Miocene reflectors still downlap the basement landward. See location in Fig. 2. Corresponding non-interpreted seismic profiles in supplementary materials (DR9).

Fig. 8. Gravity maps (Sandwell and Smith, 1997) representing main vertical motions at different periods along the FNCPA. **A.** Approximate location of subsiding pull-apart basins through the Paleogene. Transtension across the margin was ended during the Oligocene due to the change of convergence obliquity (estimated from Quinteros and Sobolev, 2013; based on Müller et al., 2008). **B.** Regional subsidence affected the entire margin during early Miocene. Compressional event allowed the uplift of the OFH as soon as the end of early Miocene. **C.** Due to basal erosion and uplift of the MDZ, a localized basin appeared between the MDZ and the continent (here called the eastern depocenter). Uplift ceased around Pleistocene between 8-10°S and continued to recently north of 8°S.

Fig. 9. Cartoons of the architecture of the FNCPA showing the main aspects discussed in this study. **A.** Significant uplift at the MDZ. **B.** Weak uplift at the MDZ.

CRediT author statement

Marie C. Genge: Conceptualization, Investigation, Writing – Original Draft, Visualization
Cesar Witt: Conceptualization, Writing – Review & Editing, Supervision, Funding acquisition
Frank Chanier: Writing – Review & Editing, Validation
Jean-Yves Reynaud: Writing – Review & Editing, Validation
Ysabel Calderon: Resources, Conceptualization, Review & Editing

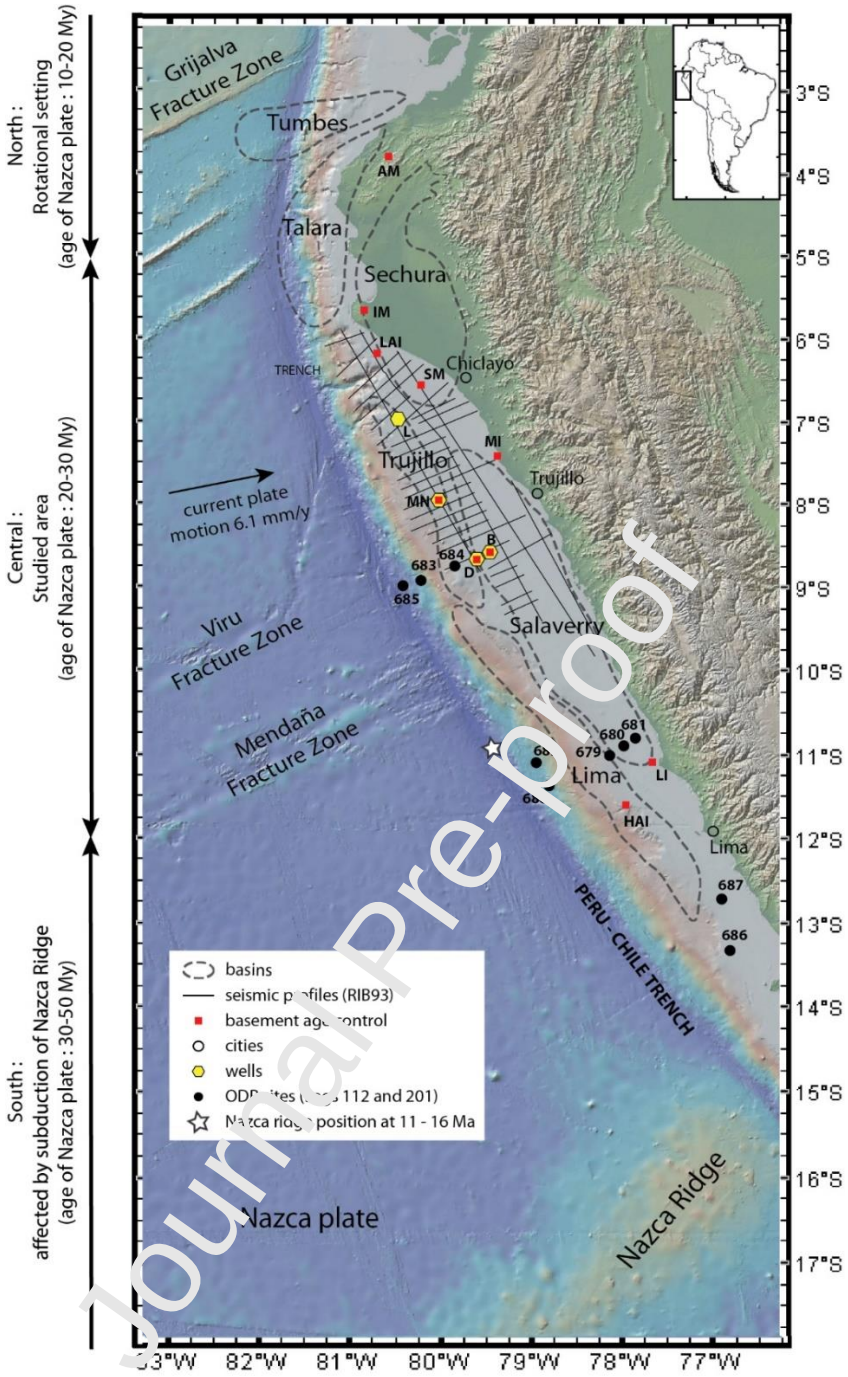

Figure 1. Geodynamic sketch of North and Central Peru showing the location of seismic lines used in this study. Black circles show ODP sites from Leg 112 and 201 (sites' number indicated on the map). Yellow hexagons show industrial well sites (B: Ballena 1X, D: Delfin 1X, L: Lobos 1X, MN: Morsa Norte 1X). Red rectangles refer to obtained basement ages discussed in the text (AM: Amotapes Massif, HAI: Homigas de Afuera Island, IM: Illescas Massif, LAI: Lobos de Afuera Island, LI: Lobera Island, MI: Macabi Island, SM: San Martin 1X). Basins boundaries were obtained from Perupetro. Plate ages obtained from Müller et al. (1997). Current plate motion estimated from the Nazca-South America convergence pole of the NUVEL-1 global plate of motion model (DeMets et al., 1994). Topography and bathymetry from GeoMapApp.

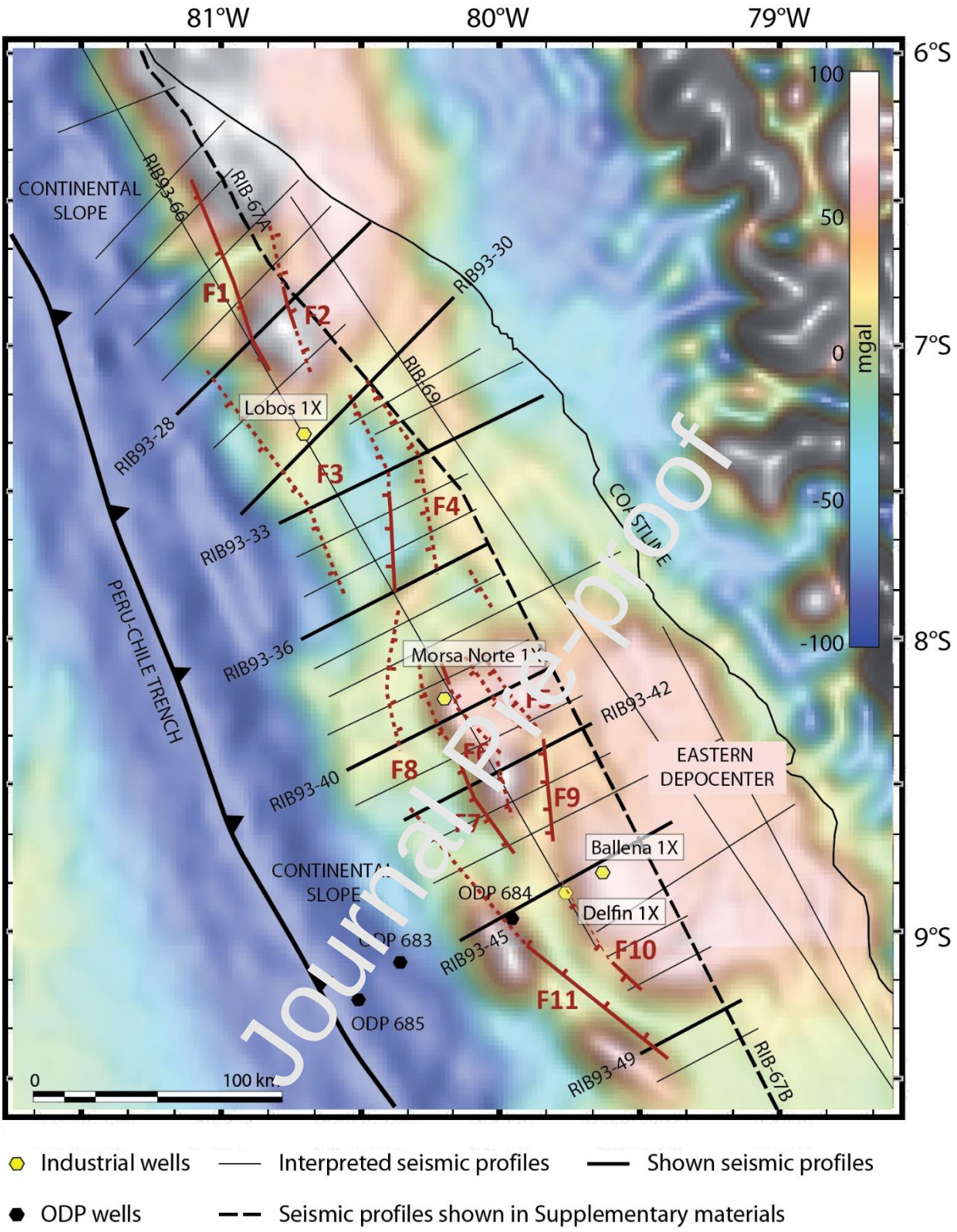

Figure 2. Gravity map (Sandwell and Smith, 1997) from GeoMapApp (resolution: 1,75 km²) with the position of seismic lines interpreted in this study and wells used for chronology purposes (PARSEP, 2001). Faults are located after seismic interpretation.

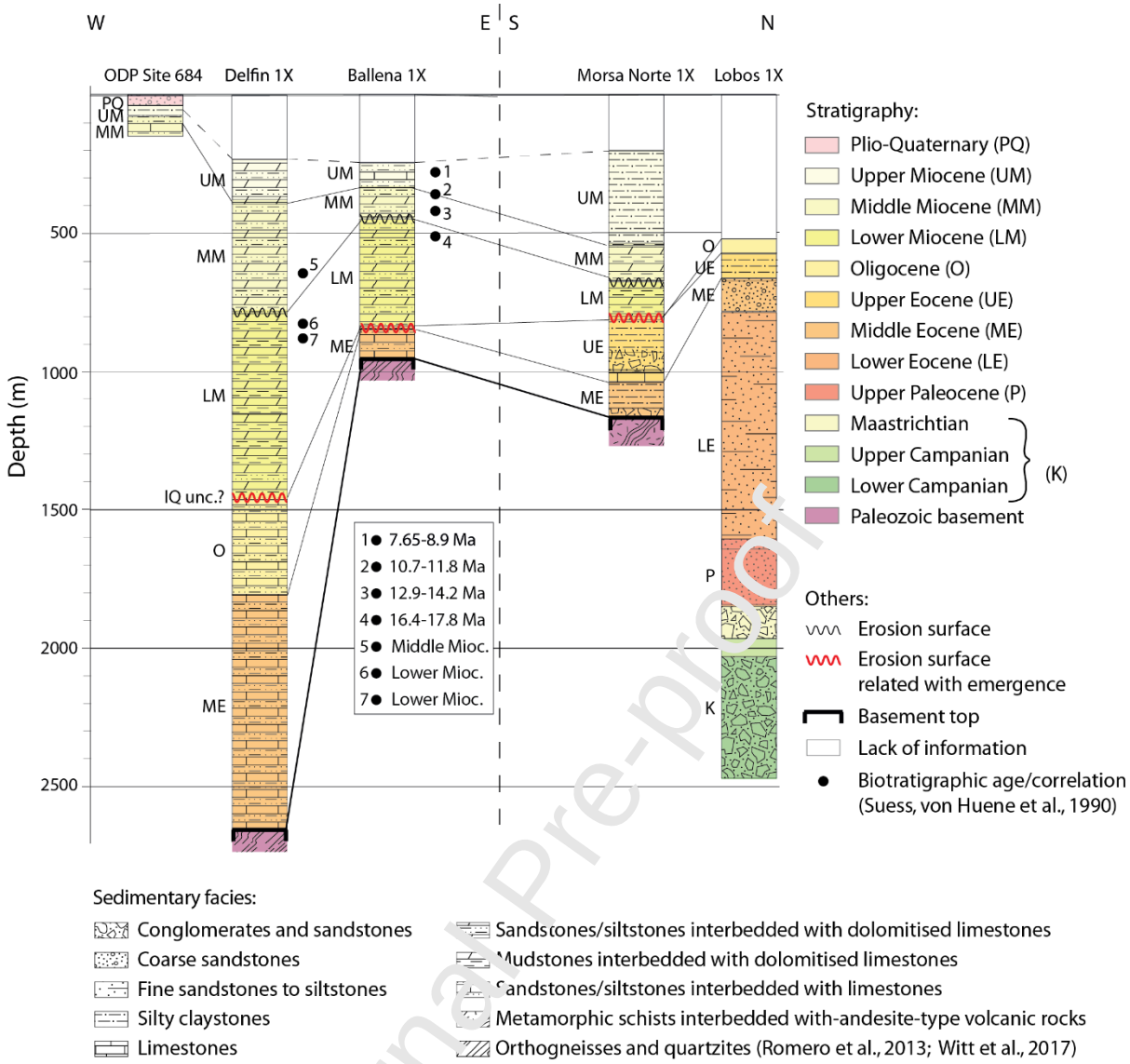

Figure 3. Log of wells used for stratigraphic correlation and basement top location (Suess, Von Huene et al., 1990; Suess and Von Huene, 1988; PARSEP, 2001).

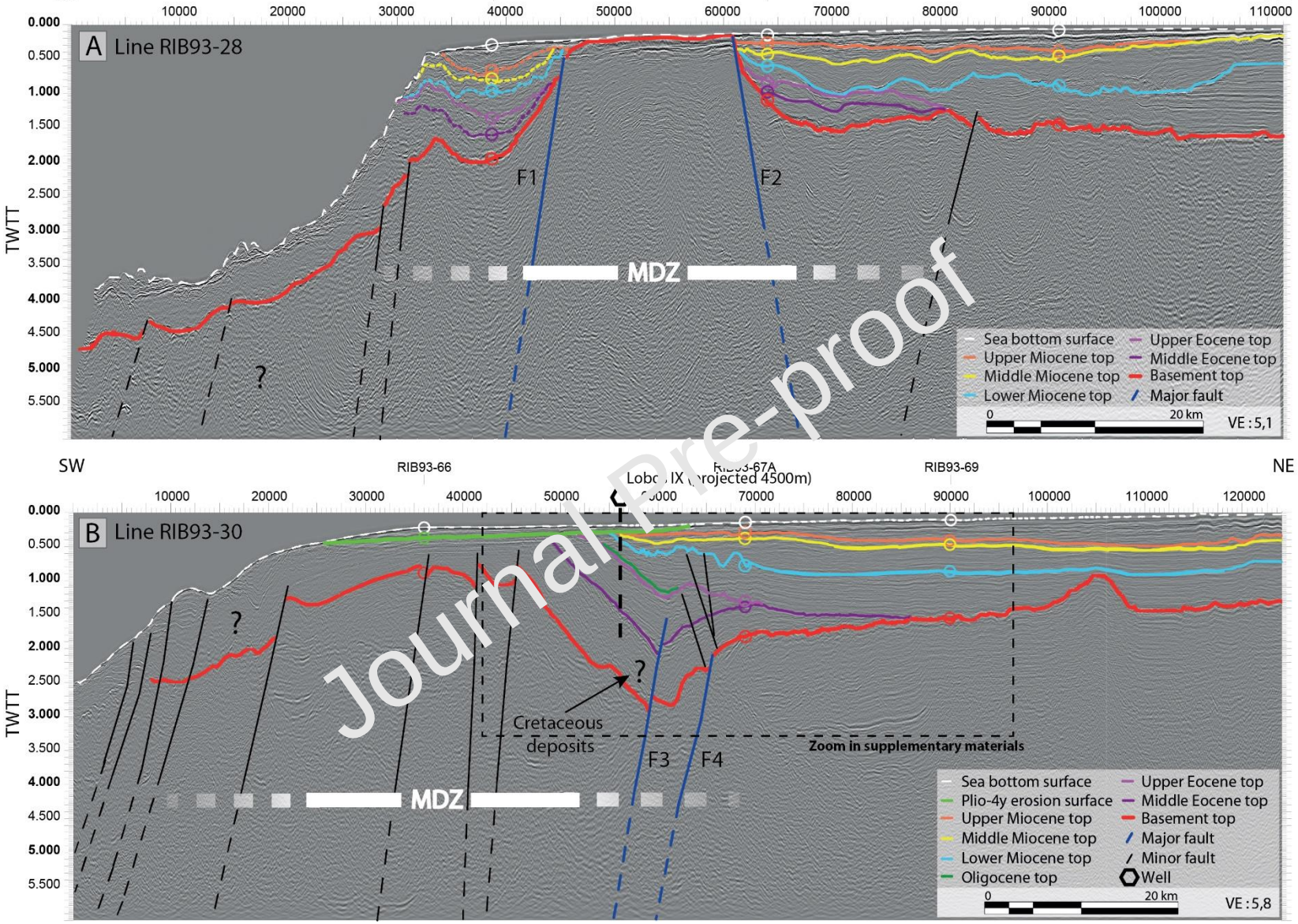

Figure 4. A. Seismic profile RIB93-28. Note the erosional slope and the near-edge basement horst. The units are folded against the faults, with an upward decreasing dip. **B.** Seismic profile RIB93-30. The basement high is buried below tilted Paleogene units covered unconformably by Plio-Quaternary deposits near the surface. Dotted square indicates the area zoomed in the supplementary materials (DR4A). See location in Fig. 2. Corresponding non-interpreted seismic profiles in supplementary materials (DR6).

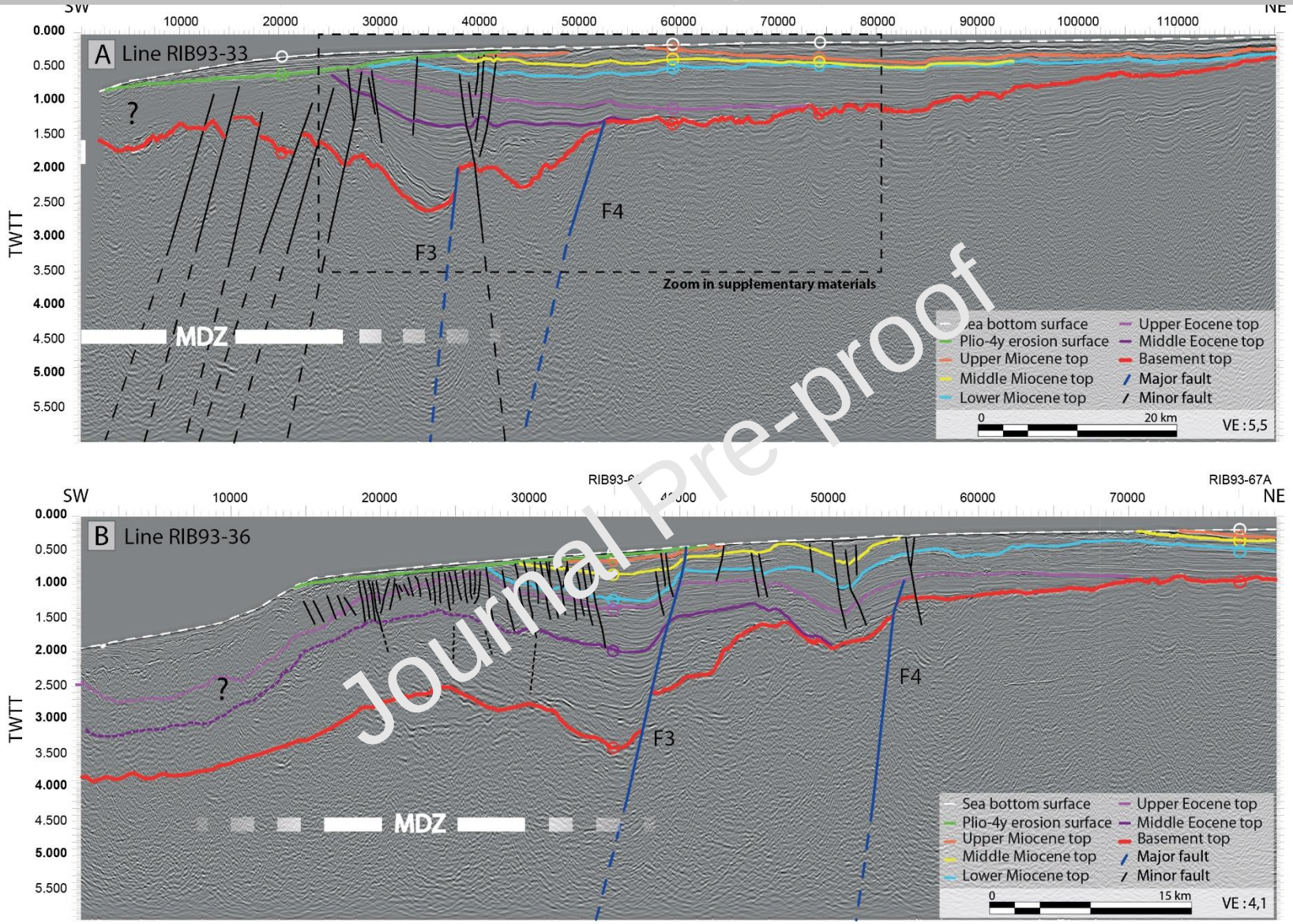

Figure 5. A. Seismic profile RIB93-33. The basement high is buried by Paleogene units below a major unconformity. Neogene deposits related with a transgression onlap the basement landward. Dotted square indicates the area zoomed in the supplementary materials (DR4B). **B.** Seismic profile RIB93-36. The basement high has a lower amplitude and is buried under Cenozoic deposits. See location in Fig. 2. Corresponding non-interpreted seismic profiles in supplementary materials (DR7).

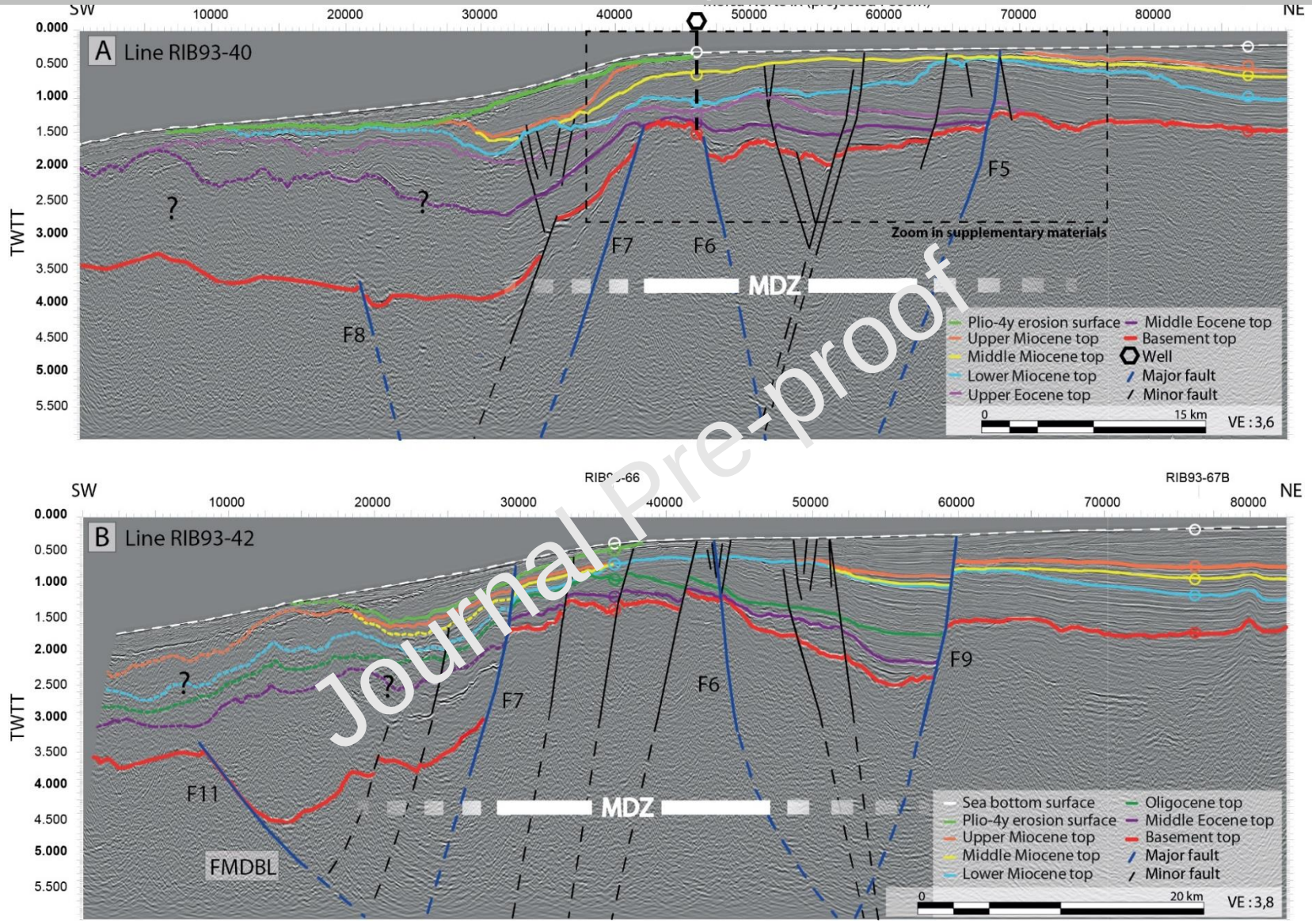

Figure 6. A. Seismic profile RIB93-40. Lower Miocene top is eroded and filled by middle and upper Miocene prograding deposits. Lower Miocene strata form apparent downlaps along the basement landward. Dotted square indicates the area zoomed in the supplementary materials (DR5A). **B.** Seismic profile RIB93-42. The fault F9 was active recently as evidence by the different thickness of Plio-Quaternary deposits on both side of the faults. FMDBL: Forward Modeling Inverse-Derived Basement Location (see Supplementary materials DR1). See location in Fig. 2. Corresponding non-interpreted seismic profiles in supplementary materials (DR8).

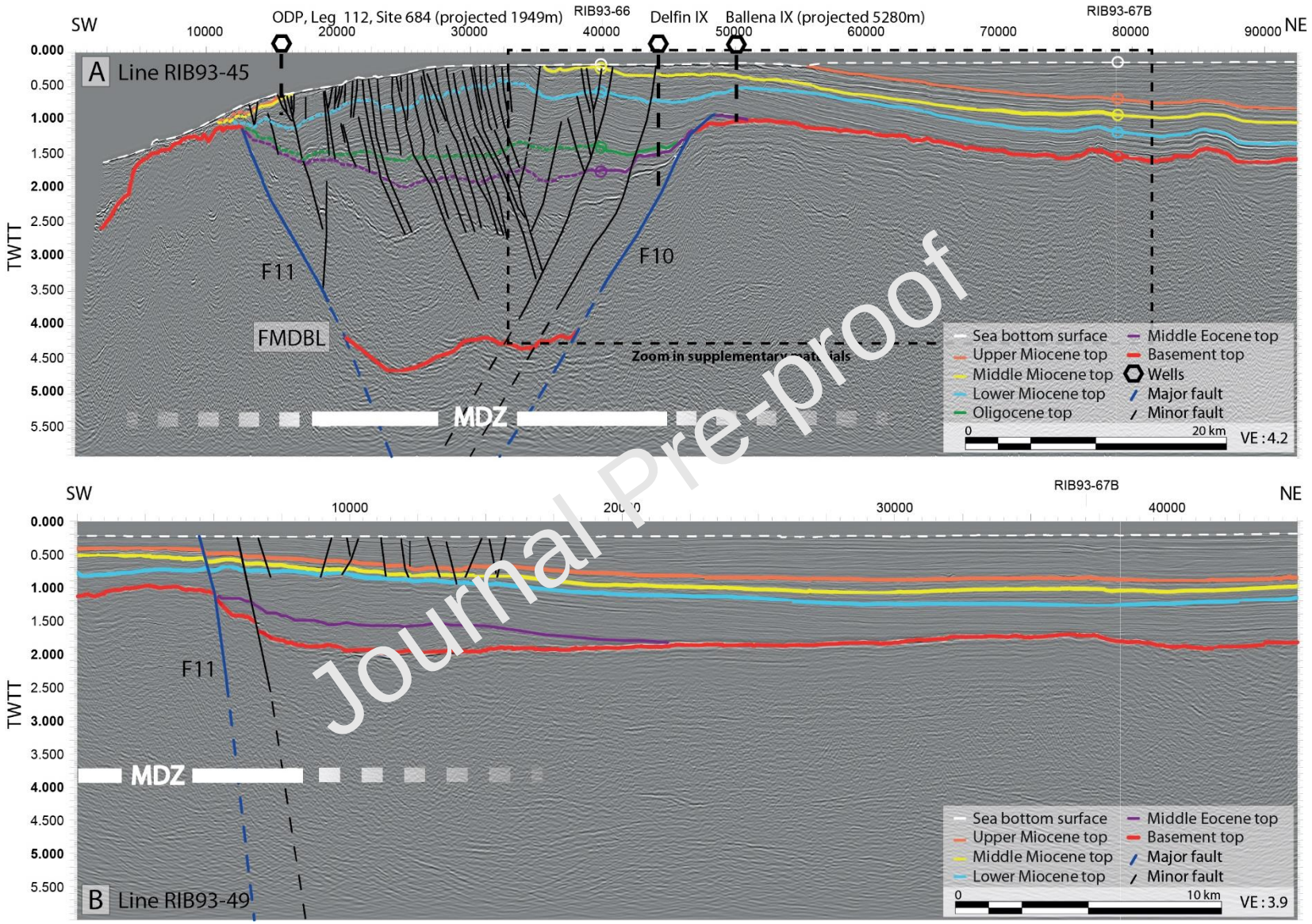

Figure 7. A. Seismic profile RIB93-45. Graben inverted during the Neogene. Landward Plio-Quaternary reflectors are tilted close to the MDZ and truncated by the current seafloor. FMDBL: Forward Modeling Inverse-Derived Basement Location (see Supplementary materials). Dotted square indicates the area zoomed in the supplementary materials (DR5B). **B.** Seismic profile RIB93-49. Lower Miocene reflectors still downlap the basement landward. See location in Fig. 2. Corresponding non-interpreted seismic profiles in supplementary materials (DR9).

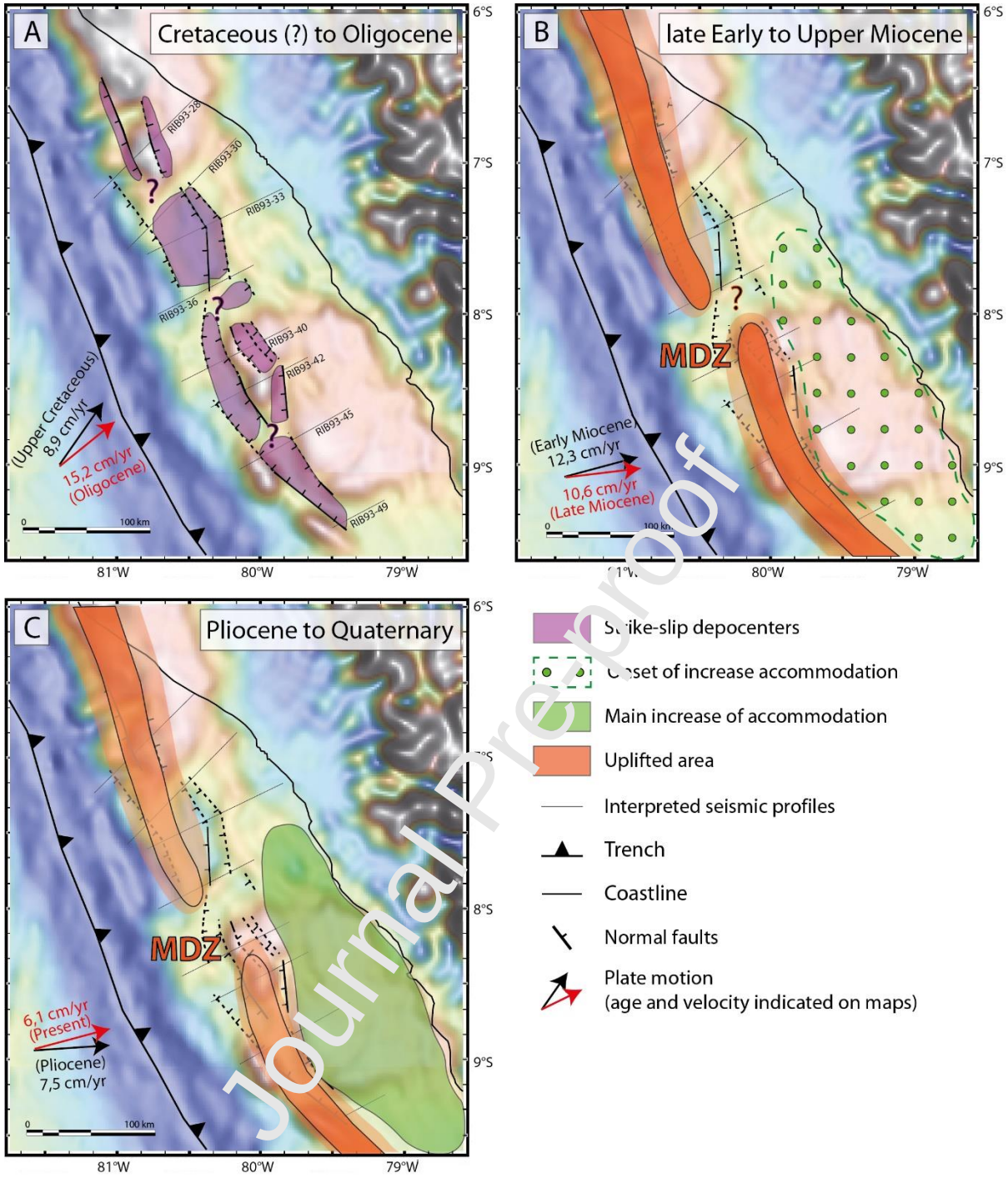

Figure 8. Gravity maps (Sandwell and Smith, 1997) representing main vertical motions at different periods along the FNCPA. **A.** Approximate location of subsiding pull-apart basins through the Paleogene. Transtension across the margin was ended during the Oligocene due to the change of convergence obliquity (estimated from Quinteros and Sobolev, 2013; based on Müller et al., 2008). **B.** Regional subsidence affected the entire margin during early Miocene. Compressional event allowed the uplift of the OFH as soon as the end of early Miocene. **C.** Due to basal erosion and uplift of the MDZ, a localized basin appeared between the MDZ and the continent (here called the eastern depocenter). Uplift ceased around Pleistocene between 8-10°S and continued to recently north of 8°S.

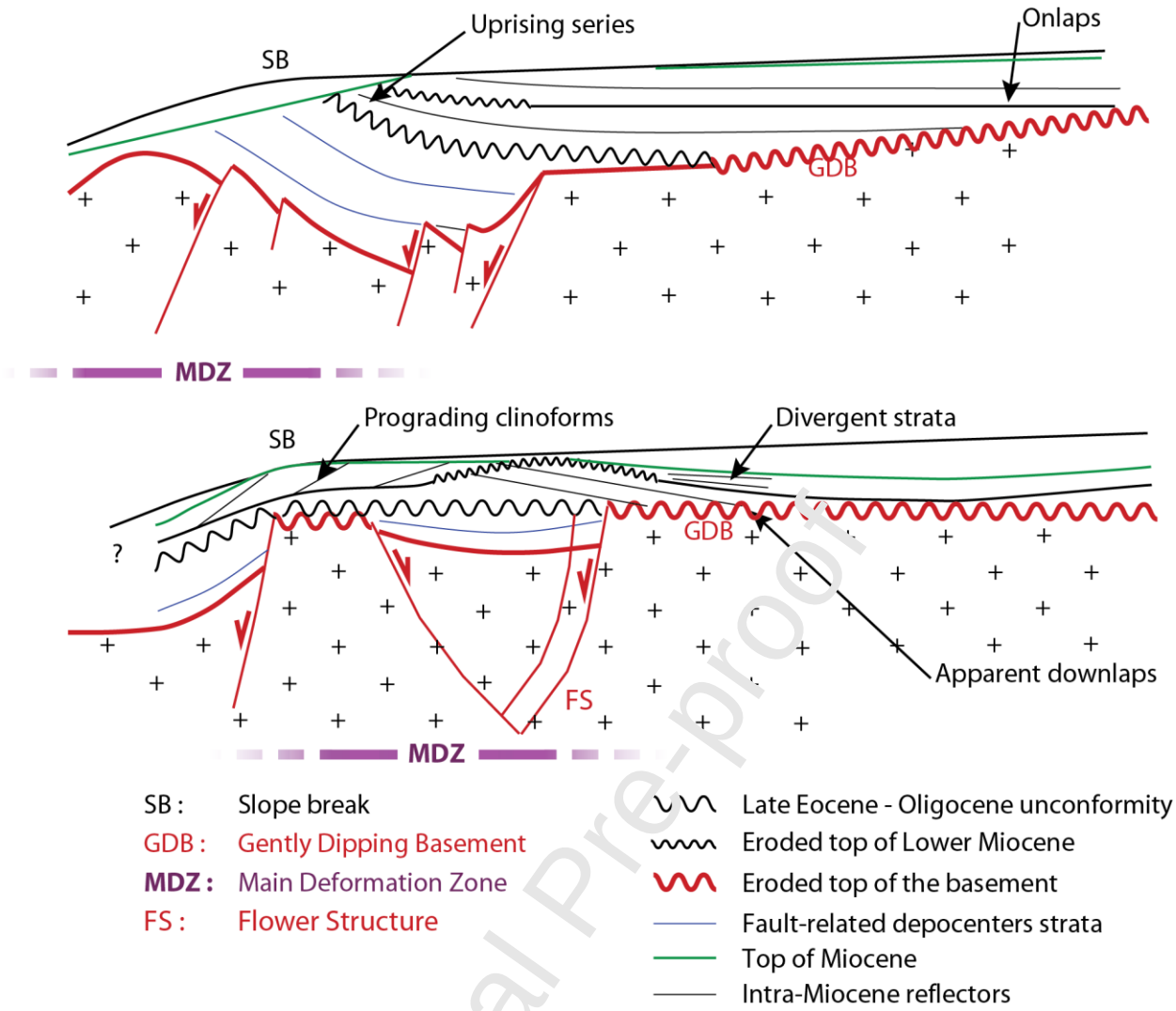

Figure 9. Cartoons of the architecture of the FNCPA showing the main aspects discussed in this study. **A.** Significant uplift at the MDZ. **B.** Weak uplift at the MDZ.

Highlights

Transtensional depocenters resulted from high obliquity convergence during the Paleogene.
A trench-parallel uplift affected unevenly and episodically the transtensional depocenters since middle Miocene.
Formation of an outer forearc high, similar to those of accretionary settings, individualized a depocenter throughout the Neogene.
Formation of the outer forearc high may have been induced by sediment underplating.